



Future weakening of southeastern tropical Atlantic Ocean interannual sea surface temperature variability in a global climate model

Arthur Prigent^{1,2} · Rodrigue Anicet Imbol Koungue¹ · Joke F. Lübbecke¹ · Peter Brandt^{1,3} · Jan Harlaß¹ · Mojib Latif^{1,3}

Received: 4 April 2023 / Accepted: 24 October 2023 / Published online: 17 November 2023
© The Author(s) 2023

Abstract

Future changes in the southeastern tropical Atlantic interannual sea surface temperature (SST) variability in response to increasing greenhouse gas concentrations are investigated utilizing the global climate model FOCI. In that model, the Coastal Angola Benguela Area (CABA) is among the regions of the tropical Atlantic that exhibits the largest surface warming. Under the worst-case scenario of the Shared Socioeconomic Pathway 5-8.5 (SSP5-8.5), the SST variability in the CABA decreases by about 19% in 2070–2099 relative to 1981–2010 during the model’s peak interannual variability season May–June–July (MJJ). The weakening of the MJJ interannual temperature variability spans the upper 40 m of the ocean along the Angolan and Namibian coasts. The reduction in variability appears to be related to a diminished surface-layer temperature response to thermocline-depth variations, i.e., a weaker thermocline feedback, which is linked to changes in the mean vertical temperature gradient. Despite improvements made by embedding a high-resolution nest in the ocean a significant SST bias remains, which might have implications for the results.

1 Introduction

Tropical Atlantic sea surface temperatures (SSTs) are marked by a strong seasonal cycle with warmest SSTs in March–April–May (MAM) and coldest SSTs in July–August–September (JAS). Variations in the amplitude and phase of the seasonal cycle give rise to SST variability on various timescales, from subseasonal to decadal (Bachèlery et al. 2020; Imbol Koungue and Brandt 2021; Prigent et al. 2020a). On interannual time scales, extreme warm and cold events, termed Benguela Niños and Niñas (Shannon et al. 1986), occur off the coasts of Angola and Namibia, in particular in the Coastal Angola Benguela Area (CABA; 10° S–20° S, within 2° off the coast, Illig et al. 2020). These events are characterized by large deviations (> 3°C) from the climatology and occur irregularly every

few years. They typically peak in MAM and last a few months, and significantly impact the regional climate (Rouault et al. 2003; Hansingo and Reason 2009; Imbol Koungue et al. 2019; Koseki and Imbol Koungue 2020), as well as marine ecosystems and fisheries (Bachèlery et al. 2016a; Binet et al. 2001; Gammelsrød et al. 1998).

Benguela Niños and Niñas are mainly driven by two forcing mechanisms: (1) remote equatorial and (2) local atmospheric forcing. The remote equatorial forcing is associated with fluctuations of the trade winds over the western and central equatorial Atlantic, triggering equatorial Kelvin waves (EKWs, Illig et al. 2004). Anomalously weak (strong) equatorial wind stress force downwelling (upwelling) EKWs propagate eastward along the equator (Polo et al. 2008), and at the West African coast part of their energy is transmitted poleward as coastal trapped waves (CTWs, Clarke 1983; Illig et al. 2018a, b). Downwelling (upwelling) CTWs can trigger warm (cold) events in the CABA by deepening (shoaling) the thermocline (Bachèlery et al. 2016b, 2020; Illig et al. 2004; Imbol Koungue et al. 2017, 2019; Lübbecke et al. 2010; Imbol Koungue and Brandt 2021), generating a subsurface temperature anomaly that will influence the mixed layer through climatological upwelling and vertical mixing. CTWs may also affect the near-coastal stratification, ocean currents and biogeochemistry (Florenchie

✉ Arthur Prigent
aprigent@ictp.it

¹ GEOMAR Helmholtz Centre for Ocean Research Kiel, Kiel, Germany

² Present Address: Earth System Physics, The Abdus Salam International Centre for Theoretical Physics, Trieste, Italy

³ Faculty of Mathematics and Natural Sciences, Kiel University, Kiel, Germany

et al. 2003; Lübbecke et al. 2010; Bachèlery et al. 2016a, 2020; Rouault 2012; Rouault et al. 2018). The local atmospheric forcing includes alongshore wind modulations related to the position and strength of the South Atlantic anticyclone (Richter et al. 2010). These alongshore wind anomalies also trigger CTWs at the eastern boundary of the tropical Atlantic and modify the local currents (Junker et al. 2017). For instance, Lübbecke et al. (2019) showed that the 2016 warm event occurring in the southeastern tropical Atlantic was mainly generated by the reduction of the alongshore winds and associated local upwelling combined with other local processes such as anomalous heat fluxes, freshwater input and meridional advection.

It has been shown that the SST anomalies along the Angolan and Namibian coasts are physically connected to the SST anomalies at the equator (Hu and Huang 2007; Lübbecke et al. 2010; Illig et al. 2020; Li et al. 2023). Hu and Huang (2007) argued that the coastal warming in the Angola Benguela area (ABA, 8° E-coast, 20° S–10° S) induces low-level wind convergence over the basin, which is likely to generate westerly surface-wind anomalies along the equator one to two months later, while Lübbecke et al. (2010) emphasized the oceanic connection via the EKWs and CTWs.

The tropical Atlantic Ocean SST also exhibits a marked multidecadal variability, hindering the detection of anthropogenic influences. Tokinaga and Xie (2011) reported a decrease of the interannual variability of the equatorial Atlantic zonal SST gradient of $48 \pm 13\%$ in root-mean-square variance for 1960–1999. This weakening of the Atlantic Niño mode over the period 1960–1999 was associated with an enhanced warming trend of the SST in the eastern equatorial Atlantic. More recently, Prigent et al. (2020b) using satellite and reanalysis data found that relative to the period 1982–1999, the eastern equatorial Atlantic interannual SST variability as measured by the standard deviation in May–June–July (MJJ) during 2000–2017 has decreased by about 30%. Consistent with the strong connection between the equatorial Atlantic and the ABA, Prigent et al. (2020a) reported a similar reduction of the MAM interannual SST variability in the ABA from 1.08 ± 0.13 °C during 1982–1999 to 0.75 ± 0.11 °C during 2000–2017.

The reduction in equatorial and southeastern tropical Atlantic SST variability over the previous decades raises the question whether this trend will continue under ongoing global warming. For the equatorial Atlantic, this question has been addressed by a few recent publications (Worou et al. 2022; Crespo et al. 2022; Yang et al. 2022). These studies found a further decrease in eastern equatorial Atlantic SST variability due to a weaker Bjerknes feedback and a more stable atmosphere. However, they have not addressed the future changes in the southeastern tropical Atlantic interannual SST variability, which is the topic of this study.

Also, as the tropical Atlantic can be expected to continue to warm during this century due to increasing atmospheric greenhouse gas (GHG) concentrations (Bakun et al. 2015), the question arises if the interannual SST variability in the southeastern tropical Atlantic will also change in the future, and if so, how is it going to change. The answer to this question might be ambiguous considered the major events in the equatorial and eastern tropical Atlantic that occurred during recent few years (Richter et al. 2022; Li et al. 2023; Imbol Koungue et al. 2021; Brandt et al. 2023). In this study, we address the question of the future SST variability in the southeastern tropical Atlantic by utilizing the global climate model Flexible Ocean and Climate Infrastructure (FOCI, Matthes et al. 2020) that has an embedded high-resolution nest in the tropical and South Atlantic Ocean (Schwarzkopf et al. 2019). Embedding a high-resolution nest helps to reduce the warm SST bias in the southeastern tropical Atlantic Ocean, yet a significant bias remains and might impact the results. We compare an ensemble of four historical simulations with an ensemble of six future simulations forced by the Shared Socioeconomic Pathway 5-8.5 (SSP5-8.5, O'Neill et al. 2016) scenario.

This paper is organized as follows. The data and methods as well as the FOCI and its validation are described in Sect. 2. Future changes in interannual SST and upper-ocean temperature variability in the southeastern tropical Atlantic are presented in Sect. 3, and the underlying mechanisms are analyzed in Sect. 4. The influences of mean-state changes on the interannual variability are discussed in Sect. 5. Section 6 provides a summary and a discussion of the main findings.

2 Data, methodology and model verification

2.1 Data

2.1.1 Observational and reanalysis datasets

For model validation, we use the SST from the fifth generation of the European Centre for Medium-range Weather Forecast (ECMWF) atmospheric reanalysis (ERA5; Hersbach et al. 2020), with $0.25^\circ \times 0.25^\circ$ horizontal resolution available for the time period January 1940 onwards. We also use the SST from the Hadley Centre Sea Ice SST data set Version 1.1 (HadISST; Rayner et al. 2003), with $1^\circ \times 1^\circ$ horizontal resolution that is available from January 1870 onwards. The Ocean Reanalysis System Version 5 (ORAS5; Zuo et al. 2019) from the ECMWF available with $0.25^\circ \times 0.25^\circ$ horizontal resolution and spanning the period January 1958 onwards is used for ocean temperature and SST. Rainfall data are taken from the Global Precipitation Climatology Project Version 2.3 (GPCP; Adler et al., 2018)

available from January 1979 to the present with $2.5^\circ \times 2.5^\circ$ horizontal resolution.

2.1.2 CMIP6 models

Output from fifteen models participating in the Coupled Model Intercomparison Project Phase 6 (CMIP6; Eyring et al. 2015; Table S1) are used to compare the performance of the FOCI in simulating the tropical Atlantic SST mean-state, seasonal cycle and interannual variability. The corresponding preindustrial control runs are used to estimate the range of internal multidecadal SST variability. Prior to all analysis, the data from the CMIP6 models were interpolated onto a $1^\circ \times 1^\circ$ horizontal grid using Climate Data Operator (CDO; Schulzweida 2022).

2.1.3 Model description and experiments

The FOCI is composed of the atmospheric model ECHAM6.3 (Stevens et al. 2013) coupled to the NEMO3.6 (Madec 2016) ocean model using the OASIS3-MCT coupler (Valcke 2013). The atmospheric component is the T63L95 setting of ECHAM6 with approximately $1.8^\circ \times 1.8^\circ$ horizontal resolution, 95 vertical hybrid sigma-pressure levels and the top at 0.01 hPa. The ocean model configuration is NEMO-ORCA05 (Biastoch et al. 2008) with a horizontal

resolution of $0.5^\circ \times 0.5^\circ$ and 46 z-levels in the vertical of which 14 levels are located in the upper 200 m. A high-resolution ocean nest with enhanced horizontal resolution of $1/10^\circ$ and the same z-levels, as that used in the host model, is embedded in the tropical and South Atlantic as well as the western Indian Ocean (70°W to 70°E , 63°S to 9°N ; Figure S1) via a two-way nesting approach (INALT10X; Schwarzkopf et al. 2019). In this approach, the nest receives boundary conditions from the host model and feeds information back. The nest enables, for example, enhanced representation of equatorial Kelvin and coastal trapped waves. The ocean temperature at the uppermost model level, located at approximately 3 m depth, is used as the SST.

The experiments used in this study are listed in Table 1. Six out of the ten model runs employing the high-resolution ocean nest include interactive atmospheric chemistry. The chemistry module is the Model for Ozone and Related Chemical Tracers (MOZART3, Kinnison et al. 2007) that is implemented in ECHAM6 (ECHAM6-HAMMOZ; Schultz et al. 2018). The simulations with and without interactive chemistry yield very similar results with respect to the tropical Atlantic climatology and variability and are used together in one ensemble. Temporal variations in solar radiation follow the CMIP6 recommendations provided by the SOLARIS-HEPPA project (Matthes et al. 2017). The future-scenario ensemble of FOCI (FOCI PROJ NEST

Table 1 Simulations with the FOCI model used in this study

Run	Time period	Configuration
<i>FOCI HIST NO-NEST ensemble</i>		
FOCI1.7-SW060	1950–2013	T63L95, Historical
FOCI1.4-SW054	1954–2013	T63L95 + MOZART3, Historical
FOCI1.4-SW064	1952–2013	T63L95 + MOZART3, Historical
FOCI1.4-SW065	1950–2013	T63L95 + MOZART3, Historical
<i>FOCI HIST NEST ensemble</i>		
FOCI1.13-II005	1951–2013	T63L95 + MOZART3 + INALT10X, Historical
FOCI1.14-II006	1951–2013	T63L95 + MOZART3 + INALT10X, Historical
FOCI1.14-II007	1951–2013	T63L95 + MOZART3 + INALT10X, Historical
FOCI171-JH015	1850–2013	T63L95 + INALT10X, Historical
<i>FOCI PROJ NEST ensemble</i>		
FOCI1.14-II010	2014–2099	T63L95 + MOZART3 + INALT10X, SSP5-8.5
FOCI1.14-II011	2014–2099	T63L95 + MOZART3 + INALT10X, SSP5-8.5
FOCI1.14-SW128	2014–2099	T63L95 + MOZART3 + INALT10X, SSP5-8.5
FOCI1.14-JH027	2011–2099	T63L95 + INALT10X, SSP5-8.5
FOCI1.14-JH037	2011–2099	T63L95 + INALT10X, SSP5-8.5
FOCI1.14-JH039	2000–2099	T63L95 + INALT10X, SSP5-8.5
<i>Pre-Industrial control run</i>		
FOCI1.3-SW038	1850–3349	T63L95, preindustrial control run under 1850 climate conditions, initialized from an ocean at rest and PHC2.1 climatology (Steele et al. 2001) for temperature and salinity

MOZART3 denotes interactive atmospheric chemistry. INALT10X indicates the use of the oceanic nest with a resolution of $1/10^\circ$. SSP5-8.5 indicates that the run is forced by the SSP5-8.5 scenario

hereafter) employs the scenario SSP5-8.5, representing the high end of the range of the future scenarios that can be considered as a worst-case scenario with a very strong increase of atmospheric GHG concentrations (O'Neill et al. 2016). For instance, the CO₂-concentration at the end of the simulations in 2100 amounts to 1135 ppm. More information on the FOCI configuration can be found in Matthes et al. (2020). The results from FOCI PROJ NEST are compared to two historical ensembles: FOCI HIST NEST and FOCI HIST NO-NEST both composed of four historical simulations employing observed external forcing for their respective periods (Table 1). Finally, the last 1000 years of a 1500-year long preindustrial control integration of FOCI performed without the ocean nest are used to estimate the internal multidecadal SST variability trends. The preindustrial control run is initialized with the PHC2.1 climatology (Steele et al. 2001) for temperature and salinity. A comparison between the historical FOCI ensembles, the CMIP6 ensemble and observations is given in Sect. 2.3.

2.2 Methodology

2.2.1 Definition of anomalies

To quantify the future changes in interannual SST variability, we compare the output of the future ensemble with that from the historical ensemble using two 30-year periods: (1) a reference period from January 1981 to December 2010 and (2) a future period from January 2070 to December 2099. Prior to all analysis, the linear trend estimated separately over each period was removed. Monthly-mean anomalies are computed by subtracting the climatological monthly-mean seasonal cycle derived separately for the two 30-year periods. The level of interannual variability is expressed by the standard deviation (σ).

2.2.2 Definition of the index regions

In this study we use the CABA region (Illig et al. 2020, blue box on Figure S1), which is a 2° fringe along the Southwest African coast from 20° S to 10° S. The CABA region is chosen instead of the often-used ABA because most of the interannual SST variability is occurring close the coast (Fig. 2). The CABA index is used to quantify the interannual SST variability associated with Benguela Niños and Niñas.

2.2.3 Thermocline and mixed layer depth definitions

The depth of the thermocline is defined as the depth of the maximum vertical temperature gradient. SSH anomalies (SSHa) are used as a proxy for thermocline depth variations to investigate the thermocline feedback as in previous studies (e.g.; Keenlyside and Latif 2007; Imbol Koungue and Brandt

2021). The mixed layer depth (MLD) is defined as the ocean depth at which the density has increased by 0.01 kg m⁻³ relative to the near-surface value at 10 m depth.

2.2.4 Brunt-Väisälä frequency calculation

To determine the stratification of the water column, the squared Brunt-Väisälä frequency (N^2) is used and expressed in terms of the vertical profiles of temperature and salinity (Maes and O'Kane 2014):

$$N^2(T, S) = -\frac{g}{\rho} \frac{\partial \rho}{\partial z} \approx \left(g\alpha \frac{\partial T}{\partial z} - g\beta \frac{\partial S}{\partial z} \right) = N_T^2(T, S) + N_S^2(T, S)$$

where:

$$N_T^2(T, S) = g\alpha \frac{\partial T}{\partial z}$$

$$N_S^2(T, S) = N^2(T, S) - N_T^2(T, S)$$

$$\alpha = -\rho^{-1} \frac{\partial \rho}{\partial T}$$

$$\beta = \rho^{-1} \frac{\partial \rho}{\partial S}$$

N_T^2 is the thermal and N_S^2 the salinity contribution, β the haline contraction coefficient, α the thermal expansion coefficient, g gravity, ρ density, T temperature, S salinity and z depth.

2.2.5 Significance of the changes

The statistical significance of the differences between the two ensembles is assessed by a two-tailed Student's *t* test at the 95% confidence level.

2.3 Model validation and comparison

A common and longstanding problem in climate models is the warm SST bias along the Southwest African coast and over the eastern and central equatorial Atlantic (e.g.; Davey et al. 2002; Richter 2015; Farneti et al. 2022). In observations, the warm poleward flowing Angola Current meets the cold equatorward flowing Benguela Current at about 16° S creating a sharp thermal front, the so-called Angola-Benguela Front (ABF green line, Fig. 1a). However, in climate models the ABF tends to be located too far south between 18° S and 19° S (Fig. 1b, c). The ensemble-mean SST biases in the CMIP6 (Fig. 1d), FOCI HIST NO-NEST (Fig. 1e) and FOCI HIST NEST (Fig. 1f) ensembles have been calculated relative to HadISST over the period 1981–2010.

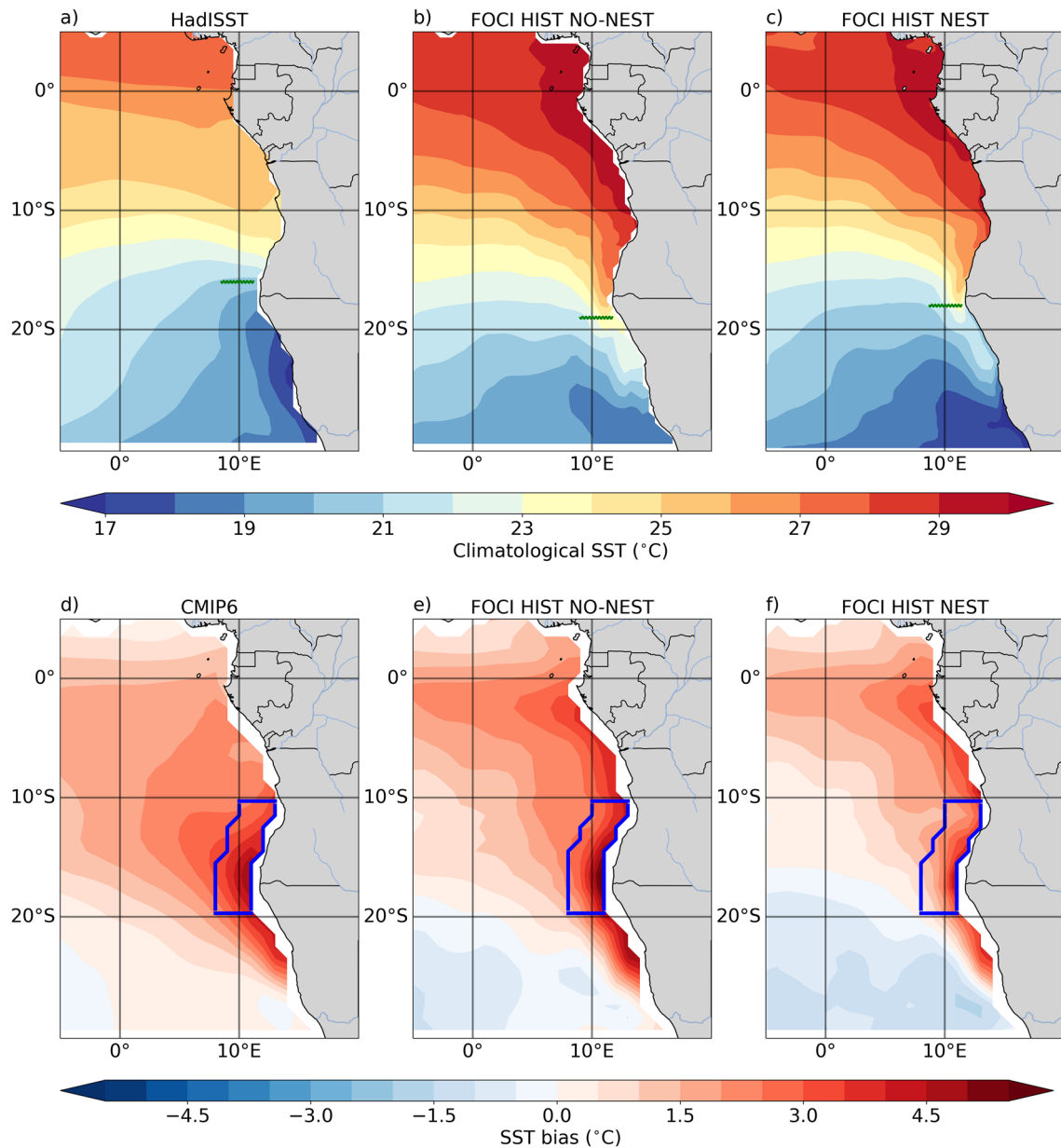


Fig. 1 Simulation of SST. **a** Mean SST from HadISST over the period 1981–2010. **b** Same as **a** but for the FOCI HIST NO-NEST ensemble mean. **c** Same as **a** but for the FOCI HIST NEST ensemble mean. **d** CMIP6 ensemble mean minus HadISST (1981–2010), **e** FOCI HIST NO-NEST ensemble mean minus HadISST (1981–2010).

f FOCI HIST NEST ensemble mean minus HadISST (1981–2010). The position of the maximum meridional SST gradient as a measure of the ABF is indicated by the green line in **a–c**. In **d–f**, the ensemble means and HadISST were bi-linearly interpolated onto a regular 1° by 1° grid

Compared to the CMIP6 ensemble mean (Fig. 1d), the FOCI HIST NO-NEST ensemble has a smaller SST bias in the CABA (Fig. 1e), with SST biases of 3.40 °C for the CMIP6 ensemble mean and of 3.23 °C for the FOCI HIST NO-NEST ensemble mean. Using the high-resolution nest in FOCI HIST NEST considerably reduces the SST bias in the CABA to 2.07 °C (Fig. 1f). This agrees with the findings of de la Vara et al. (2020) that a sole refinement of the oceanic grid reduces the warm bias further in comparison to only

increasing the atmospheric resolution in a coupled model. Yet considerable SST biases remain in the southeastern tropical Atlantic, especially in the eastern equatorial Atlantic off the South African coast, exceeding that in CMIP6 models (Fig. 1f). The remaining SST biases could be due to too coarse atmospheric resolution (approximately 1.8° × 1.8°), causing flawed near-coastal low-level winds and wind-stress curl (Harlaß et al. 2018; de la Vara et al. 2020; Kurian et al. 2021), underestimation of low-level marine stratus clouds

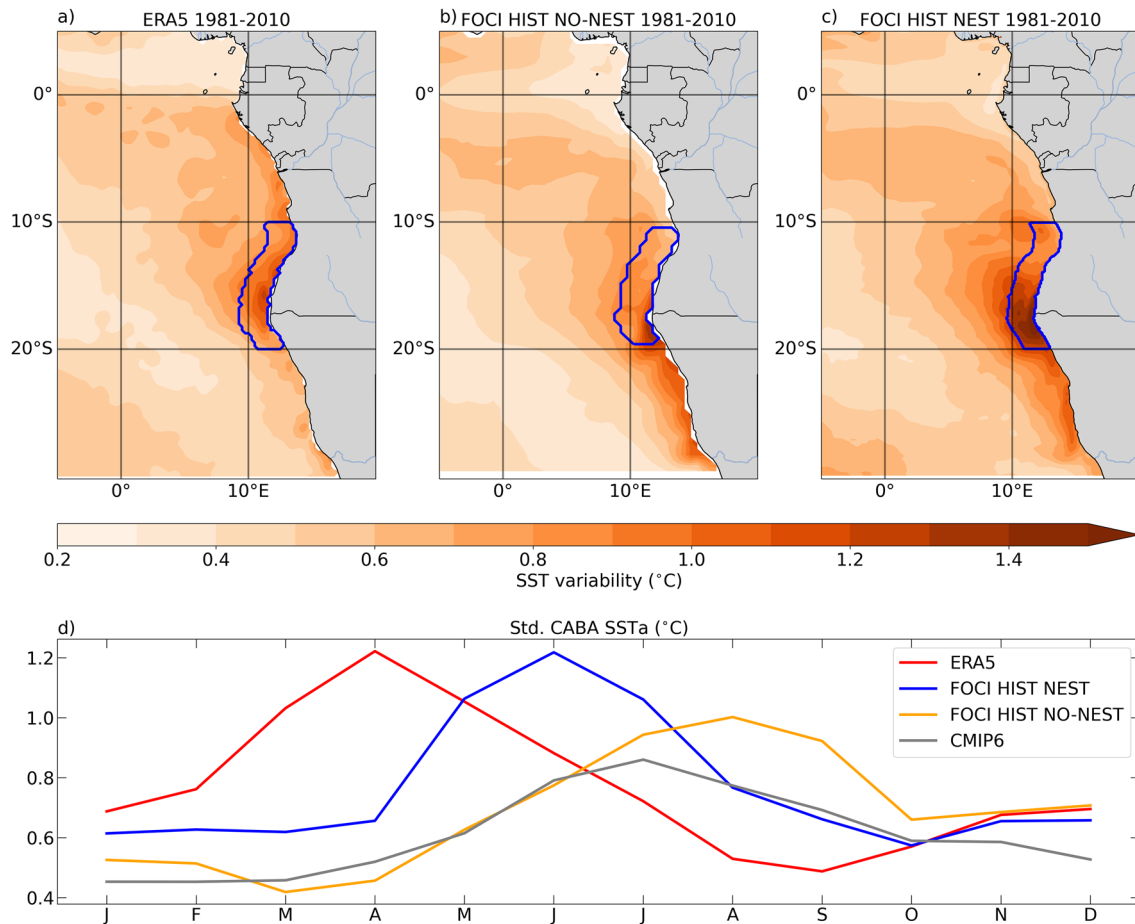


Fig. 2 **a** Standard deviation of the SSTa over the southeastern tropical Atlantic (5° W–20° E, 30° S–5° N) calculated from ERA5. **b**, **c** Same as **a** but from the FOCI HIST NO-NEST and FOCI HIST NEST ensemble means, respectively. The CABA region is denoted by the

blue box. **d** Seasonal cycle of the standard deviation of the CABA-averaged SSTa plotted as a function of the calendar month during 1981–2010 for ERA5 (red), the FOCI HIST NEST (blue), FOCI HIST NO-NEST (orange) and the CMIP6 ensemble means (grey)

(Wahl et al. 2011), misrepresentation of surface evaporation (Hourdin et al. 2015), and too weak oceanic upwelling (Small et al. 2015).

Temperature biases are not restricted to the surface. The ensemble-mean upper 200 m temperature distributions along the Southwest African coast from FOCI HIST NO-NEST and FOCI HIST NEST are compared to ORA-S5 over the period 1981–2010 (Figure S2). The FOCI HIST NO-NEST (Figure S2b) and FOCI HIST NEST (Figure S2c) ensemble means feature a warm temperature bias in the upper 50 m depth relative to ORA-S5 (Figure S2a). In comparison to the FOCI HIST NO-NEST ensemble mean (Figure S2d), the temperature bias in the FOCI HIST NEST (Figure S2e) ensemble mean is smaller with temperature biases of 2.39°C and 1.04°C in the upper 50 m and from 0° S to 27° S (green boxes in Figures S2d, e), respectively. The FOCI HIST NO-NEST and FOCI HIST NEST ensemble means exhibit a too shallow (deep) mean thermocline in MJJ from about 5° S to 27° S (0° to 5° S). Relative to ORA-S5, in FOCI HIST

NEST and FOCI HIST NO-NEST the CABA-averaged mean thermocline in MJJ is 30 m too shallow.

Next, the southeastern tropical Atlantic interannual SST variability is examined by means of the standard deviation of the SSTa for all calendar months over the period 1981–2010 for ERA5 (Fig. 2a), FOCI HIST NO-NEST (Fig. 2b) and FOCI HIST NEST (Fig. 2c). ERA5 depicts high interannual SST variability in the CABA (denoted by the blue box). Both FOCI historical ensemble means depict too high interannual SST variability, particularly south of 20° S, which could be the result of the too shallow thermocline (Figure S2). In the CABA, the interannual SST variability is better captured by the FOCI HIST NEST ensemble than the FOCI HIST NO-NEST ensemble.

State-of-the-art coupled models underestimate and misrepresent the seasonality of the interannual SST variability in the southeastern tropical (Richter and Tokinaga 2020). Figure 2d shows that in ERA5, the peak variability in the CABA occurs in April whereas the CMIP6 and

FOCI ensembles fail to simulate a realistic seasonality of the CABA-averaged interannual SST variability. A lag of two to three months in the peak of the CABA-averaged SST variability is common in the coupled models (Richter and Tokinaga 2020). In the FOCI HIST NEST (FOCI HIST NO-NEST) ensemble mean, the peak of the interannual SST variability in the CABA is in June (August) (Fig. 2d). Thus, the enhanced oceanic horizontal resolution has significantly improved the seasonality of the interannual SST variability in the southeastern tropical Atlantic, with the FOCI HIST NEST ensemble mean representing a major advance upon the CMIP6 ensemble in the CABA (Fig. 2d).

The FOCI historical ensemble means of the upper 200 m temperature variability, defined as the standard deviation of the monthly mean temperature anomalies, along the Southwest African coast are compared to ORA-S5 over the period 1981–2010 (Figure S3). Relative to ORA-S5 (Figure S3a), in FOCI HIST NO-NEST (Figure S3b) and FOCI HIST NEST (Figure S3c) the temperature variability is overestimated by 0.31 °C and 0.12 °C, respectively, (underestimated by 0.10 °C and 0.03 °C, respectively) from 25 to 70 m depth (in the upper 15 m) and from 0° to 15° S (Figures S3d, e). South of 15° S the upper 50 m depth temperature variability is overestimated by 0.2 °C for both FOCI historical ensemble means. This overestimation is likely due to the too shallow thermocline. The FOCI HIST NEST ensemble better represents the temperature variability in the upper 50 m depth along the Southwest African coast from 0° S to 15° S than the FOCI HIST NO-NEST ensemble. The nested version is therefore used in the following to study future changes in the variability, keeping in mind that the results might be impacted by the remaining biases.

3 SST variability changes

In response to the rising atmospheric GHG concentrations, the tropical Atlantic Ocean in the FOCI PROJ NEST ensemble exhibits a basin-wide SST warming that is strongest in the CABA (Fig. 3). Relative to 1981–2010 (Fig. 3a), the CABA-averaged annual mean (MJJ) SST is projected to increase by 3.09 °C (2.54 °C) by 2070–2099 (Fig. 3c, d). We note that the SST seasonal cycle over the period 1981–2010 in the CABA is in phase with that derived from ERA5, but with too warm SSTs throughout the year (Fig. 3d). In addition to the strong surface warming, there is a shift of the annual minimum CABA SST from August during 1981–2010 to July in 2070–2099, which may also have implications for the variability of local marine ecosystems.

We now investigate how the interannual variability in MJJ, the peak-variability season in the FOCI, is changing under the warmer background mean state. The interannual SST variability in MJJ experiences a clear reduction from

1981–2010 (Fig. 4a) to 2070–2099 (Fig. 4b). The difference between the two periods exhibits the largest decline in the SSTa standard deviation of about 0.25 °C in the CABA (Figs. 4c, d). When considering all calendar months, the standard deviation of the CABA-averaged SSTa amounts to 0.80 ± 0.03 °C during 1981–2010 and 0.66 ± 0.02 °C during 2070–2099, corresponding to a reduction of 17.5%. In MJJ, the standard deviation of the CABA-averaged SSTa amounts to 0.98 ± 0.08 °C during 1981–2010 and 0.79 ± 0.03 °C in 2070–2099, corresponding to a reduction of 19.4%. We note that the phase of the interannual SST variability in CABA is not changing from 1981–2010 to 2070–2099 (Fig. 4d).

Changes in interannual temperature variability are not restricted to the surface (Fig. 5). The MJJ interannual temperature variability is projected to change in the upper 200 m along the Southwest African coast. During 1981–2010, strong interannual variability ($\sigma > 1.2$ °C) is simulated near the mean thermocline, reaching the mixed layer and surface along the Southwest African coast between 10° S and 20° S (Fig. 5a). During 2070–2099 (Fig. 5b) and along the Southwest African coast, the interannual variability is weakened ($\sigma < 0.15$ °C) in the upper 35 m but increased ($\sigma > 0.15$ °C) between 35 and 55 m in the latitude range 0°–15° S (Fig. 5c).

4 Mechanisms reducing the SST variability

In this section, we explore the mechanisms behind the weakening interannual SST variability off Angola and Namibia.

4.1 Role of remote and local atmospheric processes

In order to assess the role of remote and local wind stress variations for the interannual SST variability in the southeastern tropical Atlantic, we consider the regression of tropical Atlantic wind stress anomalies on CABA-averaged SSTa (Fig. 6). Relative to 1981–2010, the link between western/central equatorial zonal wind stress in April–May–June (AMJ) and Southwest African coastal SSTs in MJJ is slightly less important during 2070–2099 (Fig. 6a, b). We introduced one-month lag between the zonal wind stress anomalies and the CABA SSTa to consider the propagation time of the EKWs and subsequent CTWs. The reduction in the AMJ zonal wind stress sensitivity to CABA-averaged SSTs in MJJ is observed mainly south of the equator (~5° S). Further, there is a slightly strengthened in-phase link between CABA-averaged SSTa and (1) the near-coastal meridional wind stress anomalies (Fig. 6c, d) and (2) near-coastal wind-stress curl anomalies (Fig. 6e, f). We note that the variance explained by the CABA SST variations is small in the meridional wind stress ($R^2 < 0.2$). This suggests a somewhat stronger role of the local wind stress fluctuations in driving interannual SST variability in the CABA through

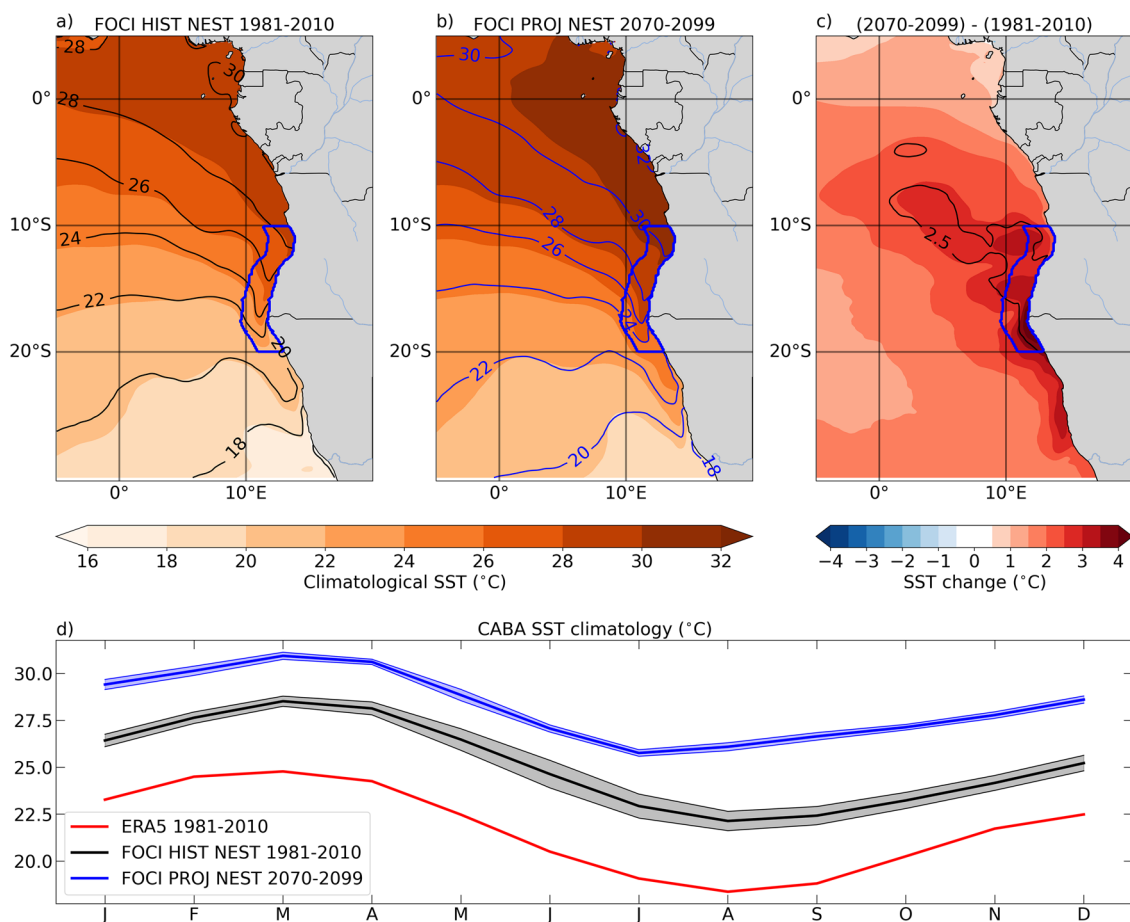


Fig. 3 Scenario-forced SST response in the FOCI model. **a** FOCI HIST NEST ensemble-mean annual mean (MJJ) SST during 1981–2010 in color (contours). **b** Same as **a** but for the FOCI PROJ NEST ensemble mean and the period 2070–2099 with blue contours for the MJJ mean. **c** Difference **b** minus **a** for all calendar month (MJJ) in color (black contours). **d** CABA-averaged SST climatology plotted as

a function of the calendar month for ERA5 for the period 1981–2010 (red line), FOCI HIST NEST for the period 1981–2010 (black line) and FOCI PROJ NEST for the period 2070–2099 (blue line). Shadings represent the FOCI ensemble spreads defined as ± 1 standard deviation of each ensemble

upwelling and/or surface heat fluxes anomalies, while the role of the zonal equatorial wind stress is almost unchanged or slightly reduced.

4.2 Role of the meridional advection

Anomalous advection along the Southwest African coast by ocean currents can also contribute to the development of Benguela Niños (Bachèlery et al. 2016b; Rouault 2012). For example, during the 2001 Benguela Niño (Rouault et al. 2007) and the 2016 warm event (Lübbecke et al. 2019) the meridional advection played an important role. To assess the role of the meridional advection, we consider the regression of the tropical Atlantic Ocean current anomalies in the upper 50 m on the CABA-averaged SSTa in MJJ (Fig. 7).

During 1981–2010 (Fig. 7a), we observe a strengthening of the South Equatorial undercurrent (SEUC) at 5° S and

from 5° W to 10° E and of the southward flowing Angola current (AC) along the Angolan coast during a warm event in the CABA in MJJ. This indicates an enhancement of the meridional advection of warm tropical waters towards the CABA during a warm event. Relative to 1981–2010, during 2070–2099 (Fig. 7b) we observe a similar pattern however with a stronger signal of the SEUC and of the AC along the Southwest African coast (Fig. 7c). This highlights a future more important role of the meridional advection in driving interannual SST variability in MJJ in the CABA.

4.3 Role of the thermocline feedback

Surface–subsurface coupling plays an important role in driving interannual SST variability in the CABA (Imbol Koungue et al. 2017; Bachèlery et al. 2020). To examine the coupling between SSTa and thermocline-depth variations,

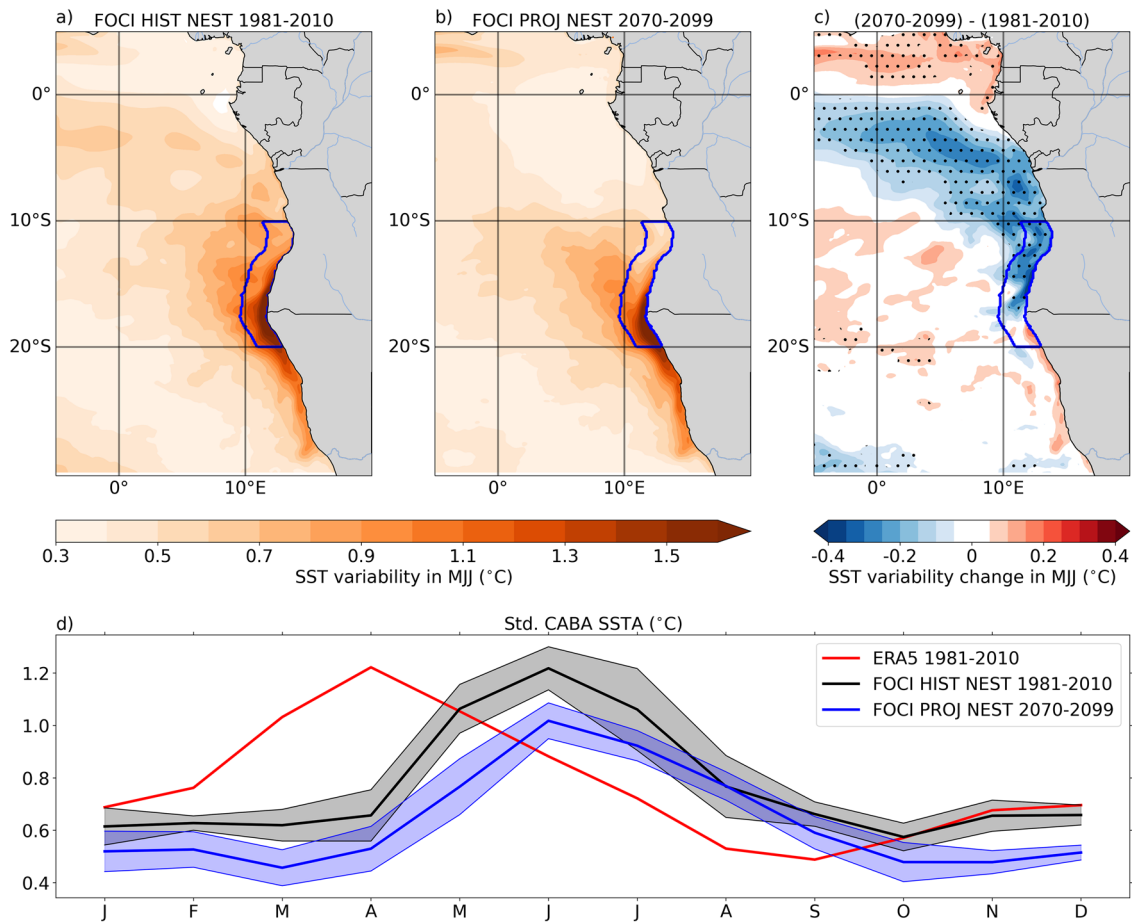


Fig. 4 Scenario-forced response in the FOCI model. **a** FOCI HIST NEST ensemble-mean standard deviation of the MJJ-averaged SSTA during 1981–2010. The blue box indicates the CABA region. **b** Same as (a) but for the FOCI PROJ NEST ensemble mean and the period 2070–2099. **c** Difference of the ensemble-mean standard deviation of the MJJ-averaged SSTA, 2070–2099 (b) minus 1981–2010 (a). Black dots indicate that the difference between the two periods is significant

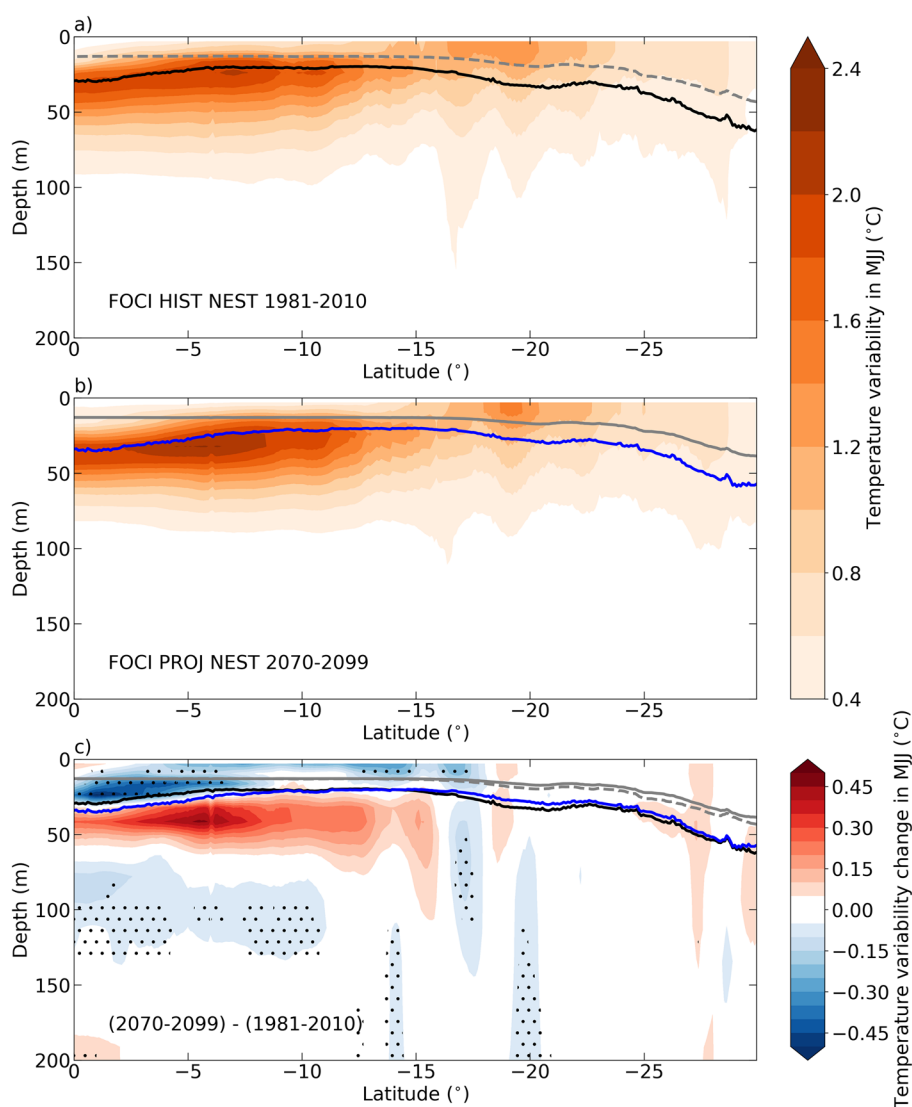
at the 95% level of a two-tailed Student’s t-test. **d** Standard deviation of the CABA-averaged SSTA plotted as a function of the calendar month for the FOCI ensemble means for the periods 1981–2010 (black line) and 2070–2099 (blue line). The red line is the standard deviation of the CABA-averaged ERA5 SSTA. The black and blue shadings represent the FOCI ensemble spread defined as ± 1 standard deviation of each ensemble

termed thermocline feedback, we pointwise regressed the MJJ SSTA on the MJJ SSHa (Fig. 8). The latter serve here as a proxy for thermocline-depth variations. During 1981–2010, large regression coefficients are observed along the Southwest African coast from 10° S to 25° S with explained variances exceeding 0.6 (Fig. 8a). We observe a similar pattern during 2070–2099 but with smaller regression coefficients and explained variances (Fig. 8b). The smaller regression coefficients illustrate a weaker SST sensitivity to thermocline perturbations in MJJ (Fig. 8c). In the CABA, the thermocline feedback estimated in this manner has reduced by 24.9%, from $35.02 \pm 3.91 \text{ }^\circ\text{C}\cdot\text{m}^{-1}$ during 1981–2010 to $26.28 \pm 2.60 \text{ }^\circ\text{C}\cdot\text{m}^{-1}$ during 2070–2099.

We next examine the regressions of the upper 200 m temperature anomalies upon the SSHa along the Southwest African coast in MJJ (Fig. 9). The SSHa are used

here again as a proxy for the thermocline-depth variations and the depth of the maximum vertical temperature gradient for the mean thermocline depth (Sect. 2.2.3). During 1981–2010, the co-variability between temperature and SSHa (Fig. 9a) is strong within about ± 20 m of the mean thermocline (black bold line). Along the Southwest African coast, large regression coefficients are found at the base of the mixed layer in the region 0° S–17° S and towards the surface in the region 17° S–23° S. During 2070–2099 (Fig. 9b), the temperature sensitivity to thermocline-depth variations has weakened between the thermocline and the base of the mixed layer along the Southwest African coast (Fig. 9c). This suggests a reduction of the effectiveness of the thermocline feedback during 2070–2099 relative to 1981–2010. The temperature sensitivity to thermocline-depth variations has

Fig. 5 Changes in interannual temperature variability in the upper 200 m. **a** Vertical section of the standard deviation (σ) of the detrended temperature anomalies in MJJ during 1981 to 2010 along the Southwest African coast (averaged within a 2° coastal band). **b** Same as **a**, but for the period 2070–2099. **c** Differences between the standard deviations during the two periods calculated as 2070–2099 (**b**) minus 1981–2010 (**a**). Black dots indicate that the difference between the two periods is significant at the 95% level of a two-tailed Student's t-test. The black (blue) solid line is the position of the MJJ mean thermocline during 1981–2010 (2070–2099). The grey lines represent the depth of the MJJ mixed layer depth for 1981–2010 (dashed line) and 2070–2099 (full line)

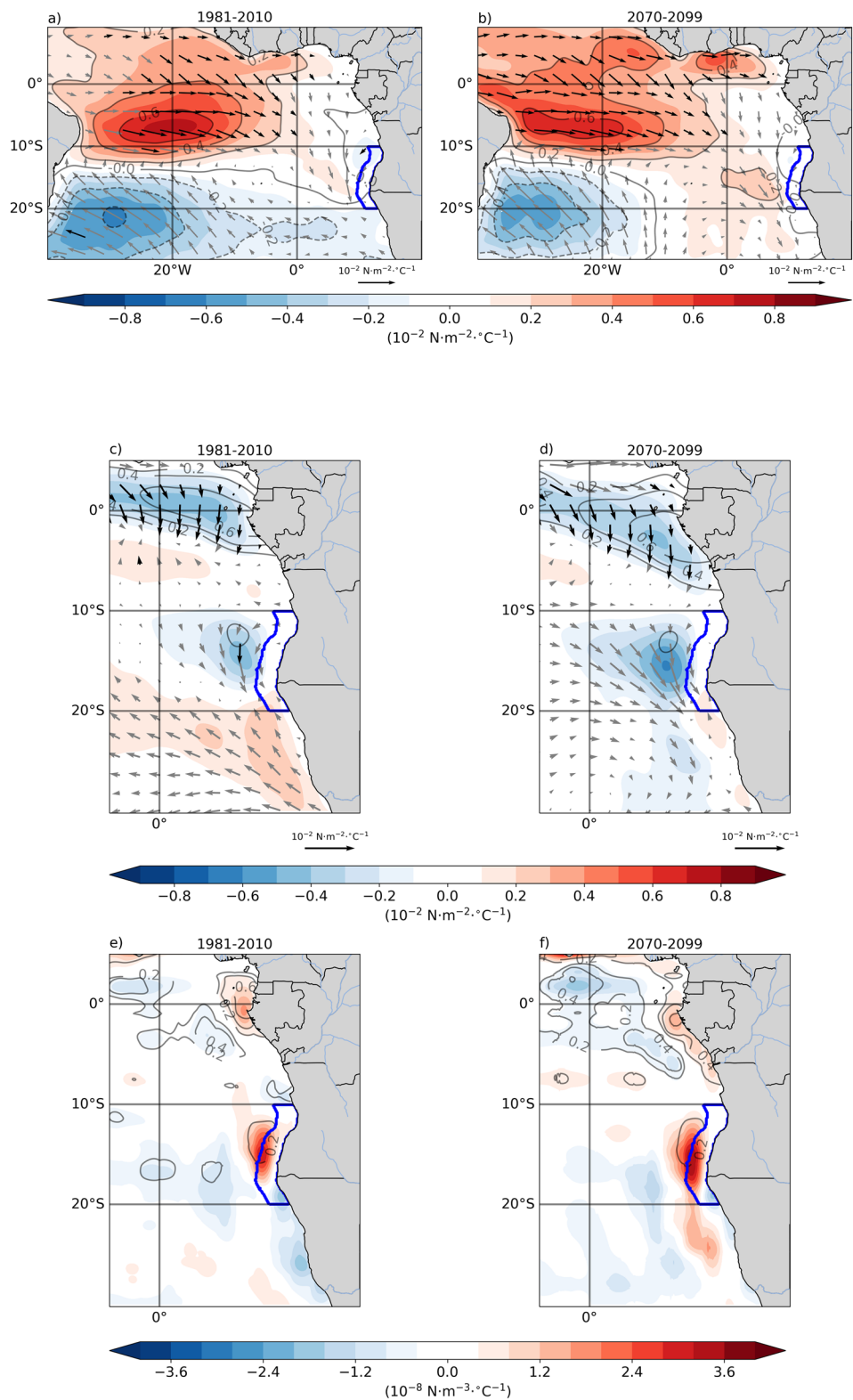


increased during 2070–2099 between 35 and 50 m depth and from 0° to 7° S (Fig. 9c). Furthermore, the increased (decreased) temperature sensitivity to thermocline variations is co-located with the increased (decreased) interannual temperature variability (Fig. 9c; thin black contours). Bachèlery et al. (2020), using model experiments, showed that equatorially forced CTWs explains up to 70% of the 0–200 m integrated temperature fluctuations in the ABA, highlighting the importance of thermocline-depth variations in driving temperature variability along the Southwest African coast. Our analysis suggests that the reduction of the interannual upper-ocean temperature variability along the Southwest African coast during 2070–2099 relative to 1981–2010 is mainly driven dynamically by the reduced SST/upper-ocean temperature sensitivity to thermocline-depth variations.

5 Influence of mean-state changes

To obtain more insight into reasons behind the changes in the thermocline feedback, we next examine the mean-state changes in MJJ along the Southwest African coast. Figure 10a, b depict the warming pattern in the upper 200 m during 2070–2099 relative to 1981–2010. The mean states in the upper 200 m for 1981–2010 and 2070–2099 are given in Figures S4 and S5, respectively. Largest warming in excess of 2.5°C occurs in the upper 50 m between 0° S and 15° S along the Southwest African coast, thereby decreasing (increasing) the magnitude of the vertical temperature gradient (dT/dz) near the surface (below the mixed layer depth; Fig. 10c, d). The changes in dT/dz

Fig. 6 Influence of wind stress and wind-stress curl anomalies on SSTa in MJJ. Ensemble-mean regressions of detrended AMJ zonal wind stress anomalies on CABA-averaged MJJ SSTa during 1981–2010 (a) and 2070–2099 (b). For the vectors, regressions have been calculated for each wind stress component separately. Black arrows indicate pointwise significant regressions for the zonal component at the 95% level. **c, d** Ensemble-mean regressions of detrended MJJ meridional wind stress anomalies on CABA-averaged MJJ SSTa during 1981–2010 (c) and 2070–2099 (d). Black arrows indicate pointwise significant regressions for the meridional component at the 95% level. **e, f** Ensemble-mean regressions of detrended MJJ wind-stress curl anomalies on CABA-averaged MJJ SSTa during 1981–2010 (e) and 2070–2099 (f)



match the changes in the thermocline feedback (Fig. 9c) and temperature variability (Fig. 5c).

Along the Southwest African coast, the ocean in the upper 25 m is becoming fresher in MJJ (Fig. 10e, f). The surface

freshening likely results from the increased precipitation over the eastern tropical Atlantic during 2070–2099 relative to 1981–2010 (Fig. 11). In addition, the FOCI PROJ NEST ensemble mean depicts a decrease of the easterlies over the

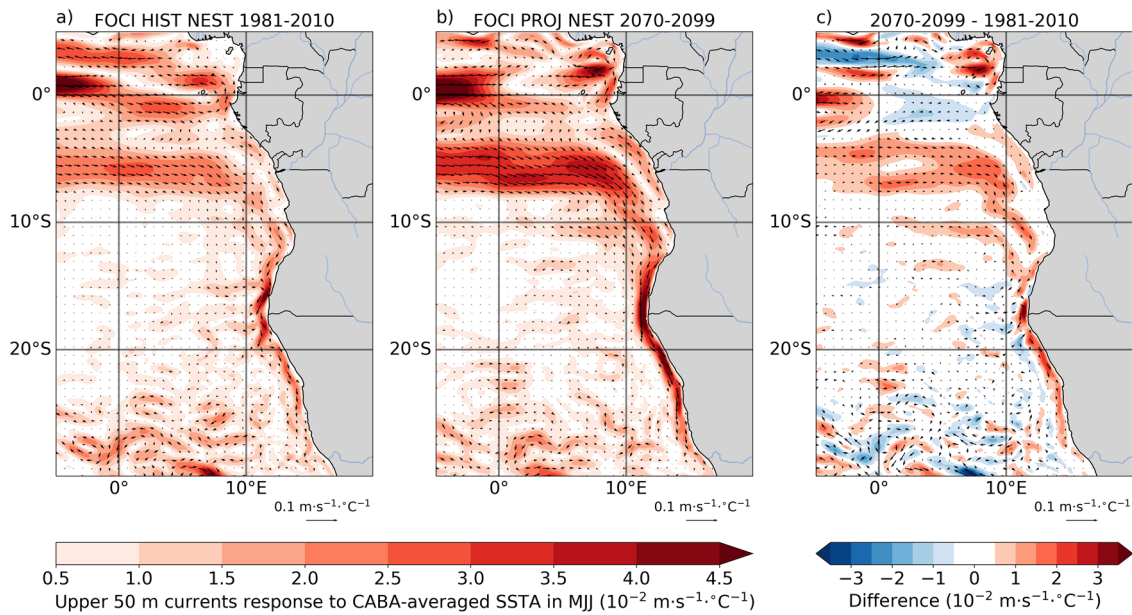


Fig. 7 Ensemble-mean upper 50 m current anomalies regression to CABA-averaged SSTa in MJJ for **a** FOCI HIST NEST during 1981–2010 and **b** FOCI HIST PROJ during 2070–2099. The shading is

the magnitude of the upper 50 m current regression. For the vectors, regressions have been calculated for each current component separately. **c** Difference **b** minus **a**

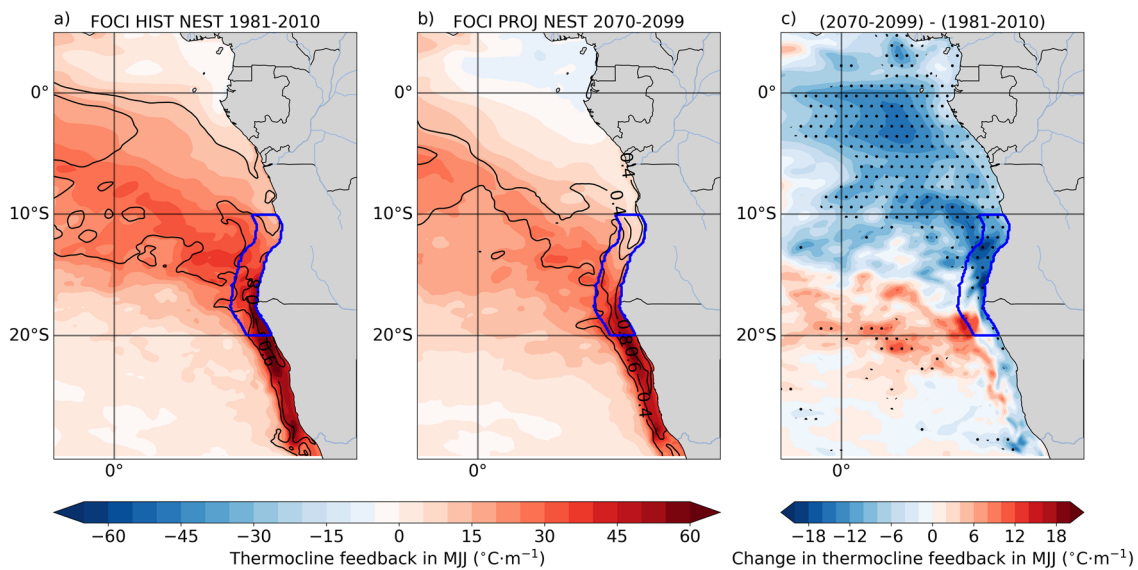


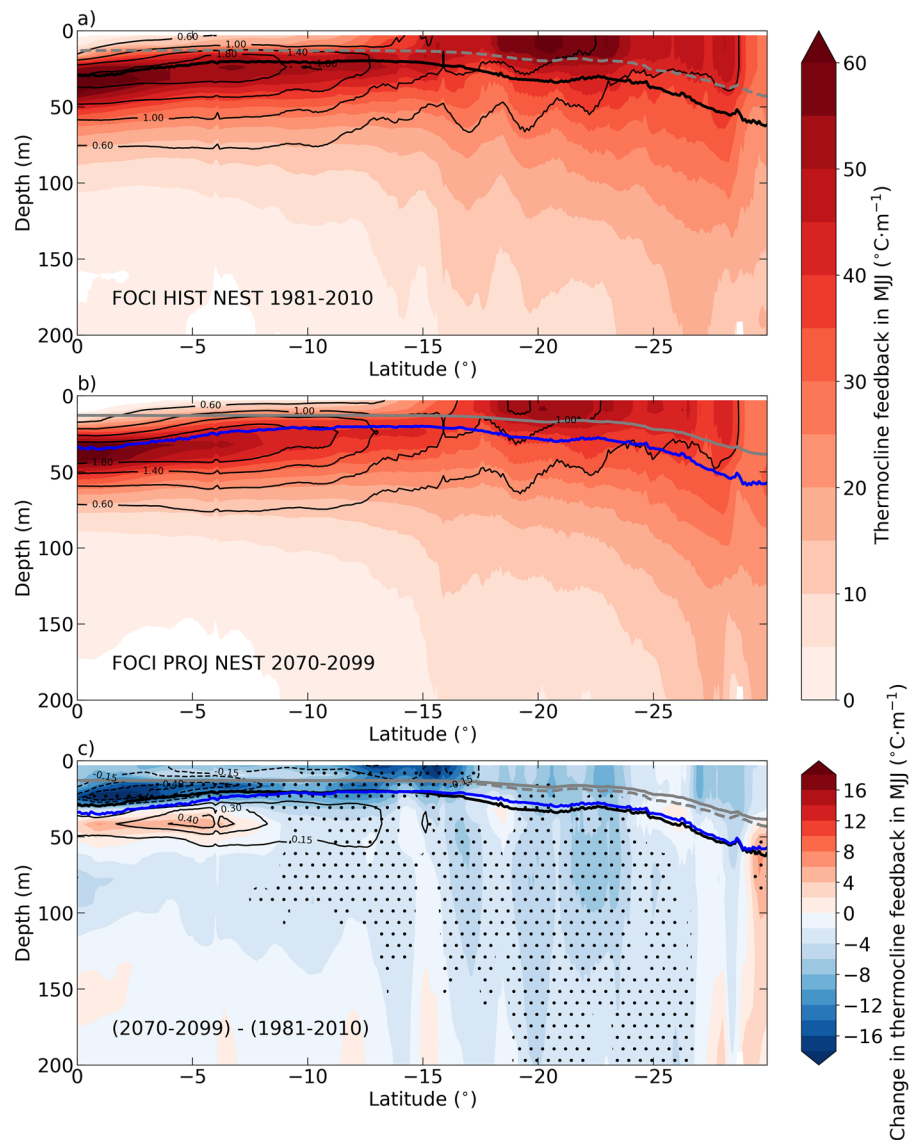
Fig. 8 Pointwise ensemble-mean regression coefficients of the SSTa on the SSHa in MJJ during **a** 1981–2010, **b** 2070–2099, and **c** their differences. Black contours in **a** and **b** indicate where the explained

variance (R^2) is 0.4, 0.6 and 0.8. Black dots indicate that the ensemble-mean change is statistically significant at the 95% level according to a two-tailed Student's *t*-test

equatorial Atlantic (Fig. 11c). These results are consistent with Park and Latif (2020), who used the Kiel Climate Model, a predecessor of the FOCI system, with a coarse-resolution ocean model ($2^\circ \times 0.5^\circ$ in the equatorial oceans) coupled to ECHAM5 at two different resolutions (T42L31 and T255L62). The temperature changes (Fig. 10a, b) act to increase the

stratification (Fig. 10g, h) through an increase of the thermal stratification (N_T^2 , Figure S6) at and below the thermocline along the Southwest African coast between 0° and 10° S. This tends to increase the interannual temperature variability there (Fig. 5c). Yang et al. (2022) showed that the CMIP6 models that projected an increase of the vertical temperature gradient

Fig. 9 Role of thermocline-depth variations in upper-ocean temperature variability. **a** FOCI HIST NEST ensemble-mean regression coefficients in the upper 200 m of detrended temperature anomalies upon SSHa (serving as proxy for thermocline-depth variations) in MJJ during 1981–2010 along a 2° coastal band along the Southwest African coast. Black contours represent the standard deviation of the MJJ temperature anomalies. **b** Same as **a** but for the FOCI PROJ NEST and the period 2070–2099. **c** Differences between the two periods, **b** minus **a**. The black (blue) bold solid line is the mean depth of the maximum vertical temperature gradient during 1981–2010 (2070–2099) taken as a proxy for the mean thermocline depth. The grey lines represent the depth of the MJJ mixed layer depth for 1981–2010 (dashed line) and 2070–2099 (full line). Black contours in **c** represent the change in MJJ temperature variability with dashed (solid) contours showing a decrease (increase) in variability during 2070–2099 relative to 1981–2010. Black dots indicate that the ensemble-mean change is statistically significant at the 95% level



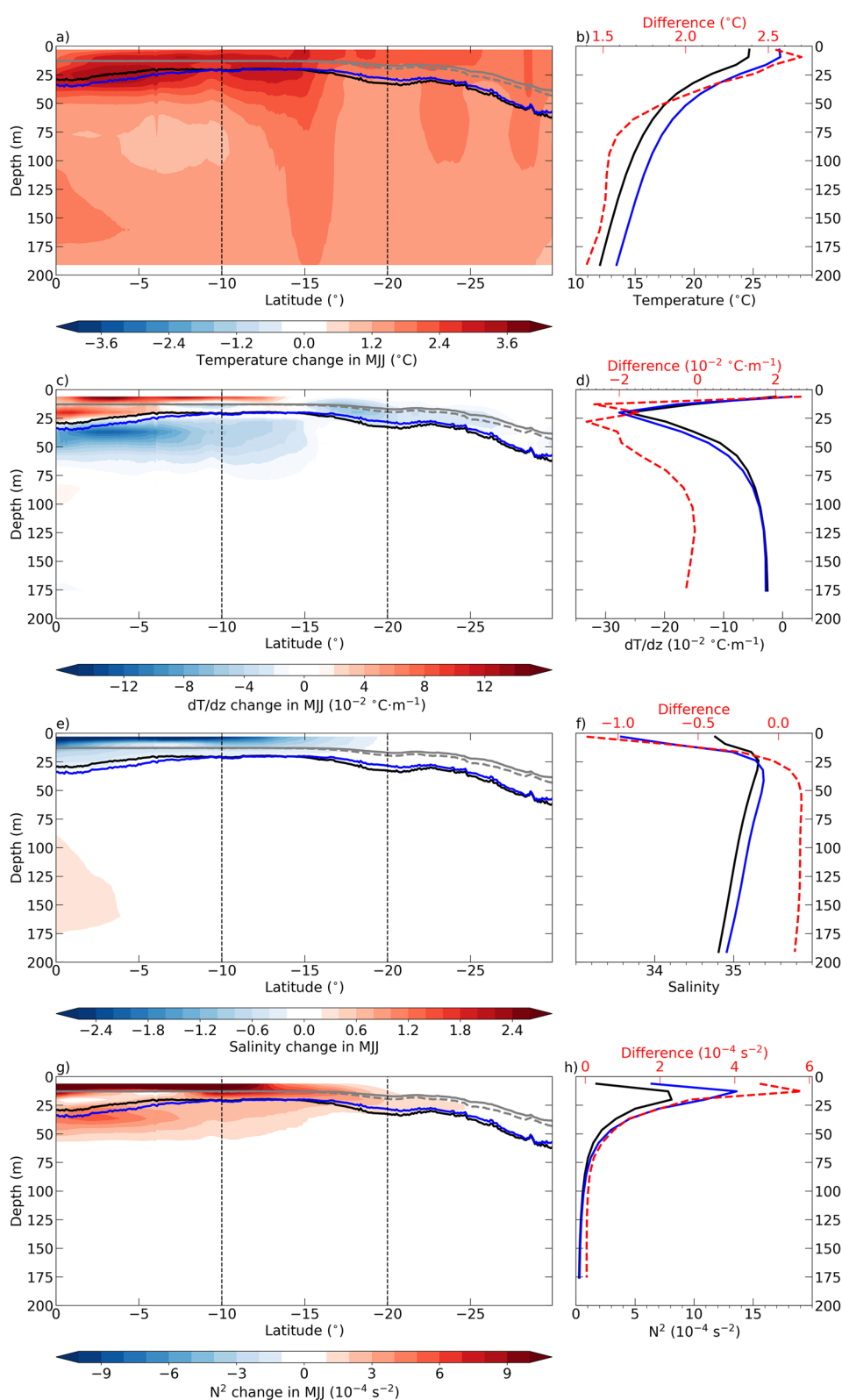
at the thermocline level in the eastern equatorial Atlantic had their SST sensitivity to SSH variations reduced (their Fig. 3b). Their findings are consistent with what we observe in the FOCI along the Southwest African coast (Fig. 8). The salinity changes (Fig. 10e, f) further act to increase the near-surface stratification (Fig. 10g, h), which is seen in the salinity stratification (N_s^2) near the surface along the Southwest African coast from 0° S and 17° S (Figure S7). The increase in near-surface stratification favors a weaker thermocline feedback and thus reduced SST variability in the CABA, as a subsurface temperature anomaly would be communicated to the surface less efficiently.

6 Summary and discussion

In this study, we compare two ensembles of simulations performed with the global climate model FOCI, which employs a high-resolution nest in its oceanic component, to investigate potential future changes in southeastern tropical Atlantic interannual SST variability. One ensemble consists of a set of historical simulations, the other of a set of global warming simulations forced by the SSP5-8.5 scenario.

We find that relative to 1981–2010, the CABA-averaged interannual SST variability in MJJ weakens by 19.4%,

Fig. 10 Upper-ocean mean-state changes in MJJ. **a** Ensemble-mean upper-ocean (0–200 m) temperature differences in MJJ in 2070–2099 relative to 1981–2010 along a 2° coastal band along the Southwest African coast (30° S–0°). **c** Same as **a**, but for the vertical temperature gradient. **e** Same as **a**, but for the salinity. **g** Same as **a**, but for the Brunt-Väisälä frequency squared (N^2). In **a**, **c**, **e**, **g** grey lines represent the depth of the MJJ mixed layer depth for 1981–2010 (dashed lines) and 2070–2099 (full lines) and the black (blue) solid lines are the mean depth of the maximum vertical temperature gradient during 1981–2010 (2070–2099) taken as a proxy for the mean thermocline depth. **b**, **d**, **f**, **h** are CABA-averaged temperature, dT/dz , salinity and N^2 profiles for 1981–2010 (black) and 2070–2099 (blue), respectively. The red profiles denote the differences 2070–2099 minus 1981–2010. The CABA region is denoted by grey vertical dotted lines in **a**, **c**, **e**, **g**



from 0.98 ± 0.08 °C during 1981–2010, to 0.79 ± 0.03 °C in 2070–2099. Further, the interannual temperature variability reduces in the upper 35 m along the Southwest

African coast between 0° and 20° S while the variability increases between 35 and 50 m depth (Fig. 5).

Benguela Niños and Niñas are known to affect the climate of the surrounding continents, for instance the precipitation

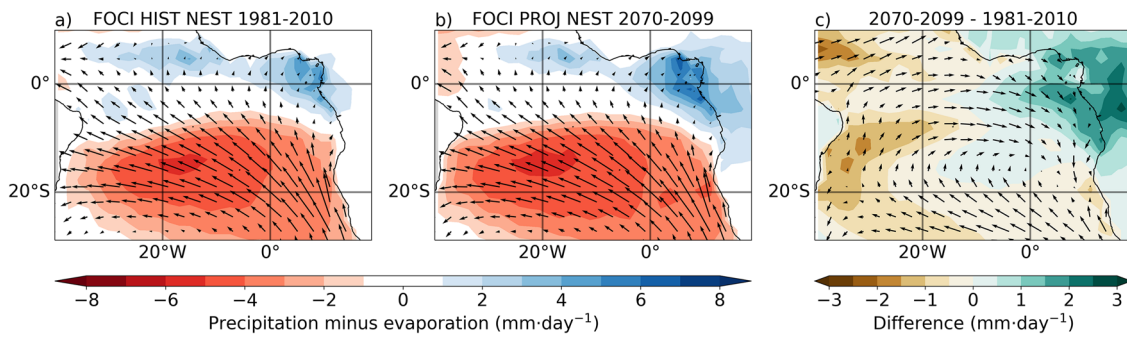


Fig. 11 Mean-state change in the modeled surface freshwater flux and surface wind stress. **a** Annual-mean precipitation minus evaporation and surface wind stress during 1981–2010. **b** Same as **a**, but for 2070–2099. **c** Differences between the two periods

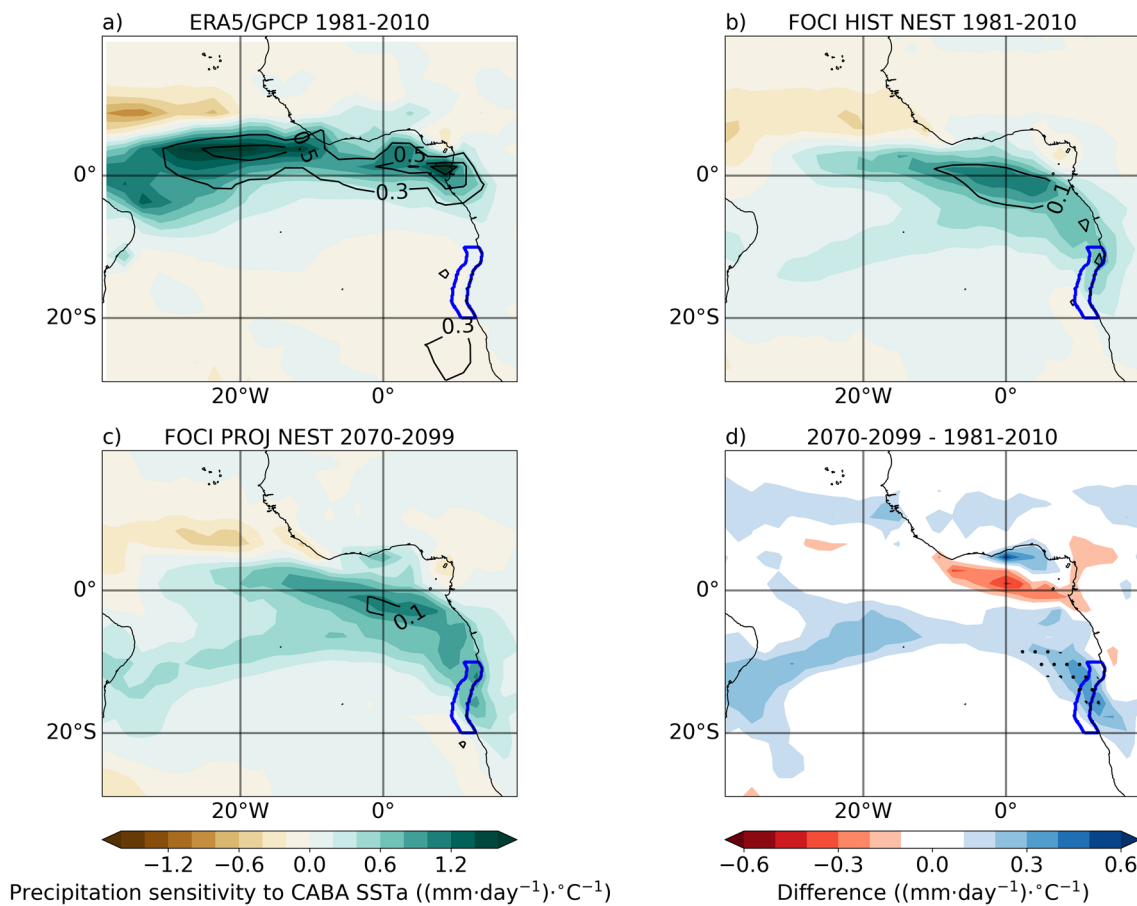


Fig. 12 Precipitation sensitivity to southeastern tropical Atlantic SST variability. **a** Linear regression of the detrended GPCP precipitation anomalies upon CABA-averaged detrended ERA5 SSTa over the period 1981–2010. **b** Same as **a**, but for the FOCI HIST NEST ensemble mean. **c** Same as **b** but for the FOCI PROJ NEST ensemble

mean and over the period 2070–2099. **d** Difference **c** minus **b**. Black contours in (**a-c**) represent the explained variance. Black dots indicate that the ensemble-mean change is statistically significant at the 95% level

(Hirst and Hastenrath 1983; Rouault et al. 2003). The precipitation regressions upon the CABA-averaged SSTa, which are influenced by Benguela Niños and Niñas, are shown for the reanalysis datasets and FOCI ensemble means in Fig. 12.

Over the period 1981–2010, the reanalysis datasets depict positive regressions over the equatorial Atlantic from 40° W to 15° E (Fig. 12a). The FOCI HIST NEST ensemble mean also depicts positive regressions over the equatorial

Atlantic (Fig. 12b). However, less variance is explained (black contours) and the regressions are mainly restricted to the eastern equatorial Atlantic (20°W–10°E). The precipitation sensitivity to CABA-averaged SSTa in FOCI PROJ NEST increases near the Angolan and Namibian coasts and decreases in the eastern equatorial Atlantic in 2070–2099 relative to 1981–2020 (Fig. 12c, d), but the regressions explain less variance in the CABA.

Both remote equatorial and local atmospheric forcing drive the interannual SST variability in the CABA (Lübbecke et al. 2010; Richter et al. 2010). The link between the western/central equatorial Atlantic zonal wind stress and CABA SSTs has slightly weakened in 2070–2099 relative to 1981–2010. On the other hand, the impact of the local along-shore wind stress on CABA SSTs has slightly increased. The influence of the meridional advection is also found to increase during 2070–2099 relative to 1981–2010. Thus, the local atmospheric wind-stress forcing and meridional advection become more important drivers of the interannual SST variability in the CABA under strongly increased GHG concentrations. These results suggest a continuation of the trend towards more locally forced Benguela Niño and Niña events that was described for the period 2000–2017 by Prigent et al. (2020a).

Regarding the local thermodynamic processes over the CABA, the net heat-flux damping as well as the cloud cover-SST feedback explain only little variance and do not exhibit large changes in the FOCI ensembles (not shown). Thus, it is unlikely that they have significantly contributed to the weakened interannual SST variability in the model.

The reduced interannual SST/upper-ocean temperature variability off the coasts of Angola and Namibia during 2070–2099 relative to 1981–2010 goes along with a reduced

SST/upper-ocean temperature sensitivity to thermocline-depth variations, i.e. a weaker thermocline feedback (Figs. 8, 9). The CABA experiences the strongest GHG-forced SST warming over the tropical Atlantic Ocean. Moreover, the subsurface temperatures in the upper 50 m from 0° S to 15° S also exhibit a substantial warming leading to a modified vertical temperature gradient (Fig. 10), which matches the changes in thermocline feedback (Fig. 9) and temperature variability (Fig. 5). In addition, the upper 25 m over the eastern equatorial Atlantic and Southwest African coast exhibit a strong freshening (Fig. 10) that likely is the result of enhanced precipitation (Fig. 11), which leads to an increase of the near-surface stratification. The increase of the near-surface stratification due to surface warming and freshening supports weaker surface/subsurface coupling or thermocline feedback. Further, the temperature changes at the thermocline level could also reduce the SST sensitivity to thermocline variations as shown by Yang et al. (2022) for the eastern equatorial Atlantic. Yet, more investigations are needed to determine the effect of vertical temperature gradient changes on the SST variability in the tropical oceans. For the tropical Pacific, Xiang et al. (2012) have suggested that a weak upper-ocean stratification decreases the thermocline-subsurface temperature feedback thereby decreasing El Niño/Southern Oscillation variability. Koyama et al. (2018) have related high thermal stratification to weaker ENSO amplitude which is consistent with the findings for the tropical Atlantic.

The 31-year running mean of the CABA-averaged SST in MJJ shows a warming trend throughout the twenty-first century (Fig. 13), while the corresponding 31-year running standard deviation of the SSTa (Fig. 13) display a downward trend. Over the 90-year period 1980–2069, the linear trend

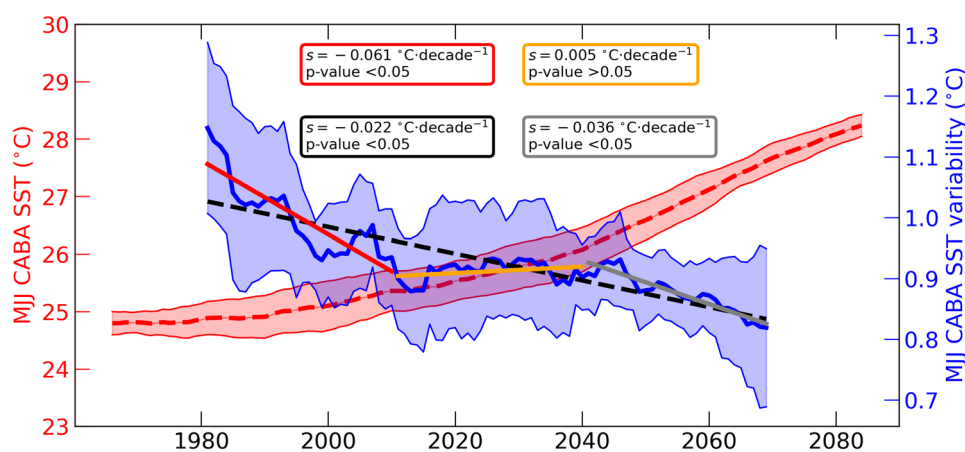


Fig. 13 CABA-averaged SST and SST variability in MJJ in the FOCI. 31-year running mean SST (red dashed line) and 31-year running standard deviation of the SSTa (blue line) for the CABA region. The shadings represent the ensemble spread defined as ± 1 standard deviation of the ensemble at each timestep. The SSTa are computed using

31-year moving baselines and linearly detrended over each window. The red, orange and grey solid lines are selected 30-year trends over the periods 1980–2009, 2010–2039 and 2040–2069, respectively to highlight the multidecadal variability

in the interannual SST variability in MJJ amounts to -0.022 °C/decade in the CABA region (Fig. 13). However, the linear trend is superimposed by a pronounced multidecadal variability, as shown by selected 30-year trends (Fig. 13). Consistent with this, a marked decadal-to-multidecadal variability has been documented in the observational record. For example, after a decadal decline of the interannual SST variability over the tropical Atlantic Ocean a resurgence of variability was observed with the 2020 and 2021 Atlantic Niños (Richter et al. 2022; Li et al. 2023) and 2019 Benguela Niño event (Imbol Koungue et al. 2021).

In order to evaluate the significance of the GHG-forced trends, we use the internal variability estimated from the pre-industrial control runs of the FOCI model and of the CMIP6 models. We note that the control run of FOCI was conducted with a model version without the high-resolution nest in the tropical and South Atlantic. Distributions of 90-year and 30-year trends in CABA-averaged MJJ-SST variability were computed from the FOCI (Fig. 14) and the CMIP6 control runs (Figure S8). The trends derived from the FOCI PROJ NEST ensemble are within the range of the trends simulated in the preindustrial control runs, suggesting that the trends in the externally forced simulations could be due to internal variability. Further, we separately compare the distributions of 90-year and 30-year trends in MJJ-SST variability when their 90-year and 30-year trends in MJJ-SST are positive or

negative to the corresponding MJJ-SST variability trends (Fig. 14). This comparison indicates that in a warming (cooling) MJJ-SST mean-state, the MJJ-SST variability is weakened (enhanced) in the FOCI and CMIP6 preindustrial control runs. Even though the long-term internal variability is large, the interannual SST variability depends on the mean state. Thus, it may be expected that the interannual SST variability in the CABA region will decrease in a warming climate.

The high level of internal variability in the FOCI and in the CMIP6 models suggests that observed multidecadal trends of the interannual SST variability in the southeastern tropical Atlantic cannot easily be linked to external forcing. For example, the reduction of the observed interannual SST variability in the ABA reported by Prigent et al. (2020a), comparing the periods 1982–1999 and 2000–2017, could be still due to internal variability.

Finally, we note some caveats about the FOCI. Despite reduced SST biases and improved representation of the seasonality of the SST variability due to the high-resolution nest in the ocean, severe mean-state and variability biases remain. For example, there is still a cold temperature bias in the western equatorial Atlantic (not shown) or a southward bias in the location of the ABF in the southeastern tropical Atlantic. This may be the result of a too coarse atmospheric resolution leading to a poor representation of the near-coastal

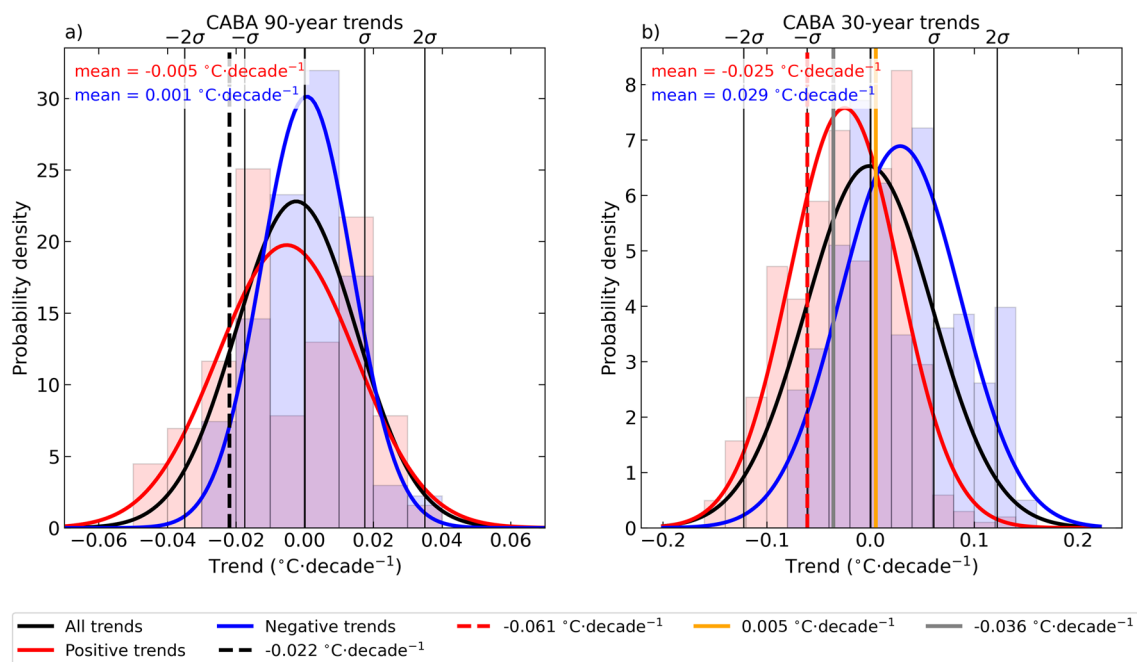


Fig. 14 Multidecadal CABA-averaged SST variability trend distributions in MJJ. **a** Distribution of 90-year CABA-averaged SST-variability trends when the 90-year CABA-averaged SST trends are positive (red) and negative (blue) calculated from the preindustrial control run with the FOCI (without the nest). **b** Same as **a** but for 30-year trends.

The vertical lines are the multidecadal trends from the FOCI ensembles shown in Fig. 13. $\pm 2\sigma$ and $\pm \sigma$ denote the two and one standard deviations of the multidecadal trend distributions, respectively. Normal distributions are defined using the mean and standard deviation of each distribution (black, red and blue curves)

and equatorial surface winds (Richter 2015; Milinski et al. 2016; Harlaß et al. 2018). Nevertheless, the SST bias in the nested version of FOCI is smaller than the averaged bias of the CMIP6 models analyzed here. This, however, does not imply that the real world will respond in the same way as suggested by the FOCI. A better understanding of the processes in the southeastern tropical Atlantic, which determine the mean state, seasonal cycle and interannual variability of the SST and upper-ocean temperature is required to further reduce model biases and in turn uncertainty regarding the externally forced climate response over the region.

Supplementary Information The online version contains supplementary material available at <https://doi.org/10.1007/s00382-023-07007-y>.

Acknowledgements We would like to thank Sebastian Wahl (GEO-MAR) for helping us to retrieve the model data. We also acknowledge the Kiel University Computing Centre for the access to high-performance computing resources.

Author contributions AP, RAIK, JFL, PB, JH and ML conceived and designed the study. Model simulations were performed by JH. Analyses were performed by AP and RAIK. The first version of the draft was written by AP and all authors commented on previous versions of the manuscript. All authors read and approved the final manuscript.

Funding Open Access funding enabled and organized by Projekt DEAL. This study was supported by the German Federal Ministry of Education and Research as part of the BANINO project (03F0795A) and by the EU H2020 under grant agreement 817578 TRIATLAS project. Rodrigue Anicet Imbol Koungue has received funding from the German Research Foundation through Grant 511812462 (IM 218/1-1).

Data availability The model data generated and analyzed during the current study are available from the corresponding author on reasonable request. The CMIP6 data can be found at <https://esgf-data.dkrz.de/search/cmip6-dkrz/>. The ERA5 data used in this study can be found at <https://cds.climate.copernicus.eu/cdsapp#!/dataset/reanalysis-era5-single-levels-monthly-means?tab=form>. The HadISST is publicly available at <https://www.metoffice.gov.uk/hadobs/hadisst/>. The GPCP data can be found at <https://psl.noaa.gov/data/gridded/data.gpcp.html>. The ORA-S5 data is available at <https://cds.climate.copernicus.eu/cdsapp#!/dataset/reanalysis-oras5?tab=form>.

Declarations

Conflict of interest The authors have no relevant financial interests to disclose.

Open Access This article is licensed under a Creative Commons Attribution 4.0 International License, which permits use, sharing, adaptation, distribution and reproduction in any medium or format, as long as you give appropriate credit to the original author(s) and the source, provide a link to the Creative Commons licence, and indicate if changes were made. The images or other third party material in this article are included in the article's Creative Commons licence, unless indicated otherwise in a credit line to the material. If material is not included in the article's Creative Commons licence and your intended use is not permitted by statutory regulation or exceeds the permitted use, you will need to obtain permission directly from the copyright holder. To view a copy of this licence, visit <http://creativecommons.org/licenses/by/4.0/>.

References

- Adler RF, Sapiano MRP, Huffman GJ, Wang J-J, Gu G, Bolvin D, Chiu L, Schneider U, Becker A, Nelkin E, Xie P, Ferraro R, Shin D-B (2018) The Global Precipitation Climatology Project (GPCP) monthly analysis (new version 2.3) and a review of 2017 global precipitation. *Atmosphere* 9:138. <https://doi.org/10.3390/atmos9040138>
- Bachèlery M-L, Illig S, Dadou I (2016a) Forcings of nutrient, oxygen, and primary production interannual variability in the southeast Atlantic Ocean. *Geophys Res Lett* 43:8617–8625. <https://doi.org/10.1002/2016GL070288>
- Bachèlery M-L, Illig S, Dadou I (2016b) Interannual variability in the South-East Atlantic Ocean, focusing on the Benguela Upwelling System: remote versus local forcing. *J Geophys Res Oceans* 121:284–310. <https://doi.org/10.1002/2015JC011168>
- Bachèlery M-L, Illig S, Rouault M (2020) Interannual coastal trapped waves in the Angola-Benguela upwelling system and Benguela Niño and Niña events. *J Mar Syst* 203:103262. <https://doi.org/10.1016/j.jmarsys.2019.103262>
- Bakun A, Black BA, Bograd SJ, Garca-Reyes M, Miller AJ, Rykaczewski RR, Sydeman WJ (2015) Anticipated effects of climate change on coastal upwelling ecosystems. *Curr Clim Change Rep* 1(2):85–93. <https://doi.org/10.1007/s40641-015-0008-4>
- Biastoch A, Böning CW, Getzlaff J, Molines J-M, Madec G (2008) Causes of interannual–decadal variability in the meridional overturning circulation of the midlatitude north Atlantic ocean. *J Clim* 21:6599–6615. <https://doi.org/10.1175/2008JCLI2404.1>
- Binet D, Gobert B, Maloueki L (2001) El Niño-like warm events in the Eastern Atlantic (6°N, 20° S) and fish availability from Congo to Angola (1964–1999). *Aquat Liv Resour* 14:99–113. [https://doi.org/10.1016/S0990-7440\(01\)01105-6](https://doi.org/10.1016/S0990-7440(01)01105-6)
- Brandt P, Alory G, Awo FM, Dengler M, Djakouré S, Imbol Koungue RA, Jouanno J, Körner M, Roch M, Rouault M (2023) Physical processes and biological productivity in the upwelling regions of the tropical Atlantic. *Ocean Sci* 19:581–601. <https://doi.org/10.5194/os-19-581-2023>
- Clarke AJ (1983) The reflection of equatorial waves from oceanic boundaries. *J Phys Oceanogr* 13(7):1193–1207. [https://doi.org/10.1175/1520-0485\(1983\)013%3c1193:TROEWF%3e2.0.CO;2](https://doi.org/10.1175/1520-0485(1983)013%3c1193:TROEWF%3e2.0.CO;2)
- Crespo LR, Prigent A, Keenlyside N et al (2022) Weakening of the Atlantic Niño variability under global warming. *Nat Clim Chang* 12:822–827. <https://doi.org/10.1038/s41558-022-01453-y>
- Davey M, Huddleston M, Sperber K et al (2002) STOIC: a study of coupled model climatology and variability in tropical ocean regions. *Clim Dyn* 18:403–420. <https://doi.org/10.1007/s00382-001-0188-6>
- de la Vara A, Cabos W, Sein DV et al (2020) On the impact of atmospheric vs oceanic resolutions on the representation of the sea surface temperature in the South Eastern Tropical Atlantic. *Clim Dyn* 54:4733–4757. <https://doi.org/10.1007/s00382-020-05256-9>
- Eyring V, Bony S, Meehl GA, Senior C, Stevens B, Stouffer RJ, Taylor KE (2015) Overview of the Coupled Model Intercomparison Project Phase 6 (CMIP6) experimental design and organisation. *Geosci Model Dev* 8(12):10539–10583. <https://doi.org/10.5194/gmdd-8-10539-2015>
- Farneti R, Stiz A, Ssebandeke JB (2022) Improvements and persistent biases in the southeast tropical Atlantic in CMIP models. *Njp Clim Atmos Sci* 5:42. <https://doi.org/10.1038/s41612-022-00264-4>
- Florenchie P, Lutjeharms JRE, Reason CJC, Masson S, Rouault M (2003) The source of Benguela Niños in the South Atlantic Ocean. *Geophys Res Lett* 30(10):1505. <https://doi.org/10.1029/2003GL017172>

- Gammelsrød T, Bartholomae CH, Boyer DC, Filipe VLL, O'Toole MJ (1998) Intrusion of warm surface layer along the Angolan-Namibian coast in February–March: the 1995 Benguela Niño. *S Afr J Mar Sci* 19:41–56. <https://doi.org/10.2989/025776198784126719>
- Hansingo K, Reason CJC (2009) Modelling the atmospheric response over southern Africa to SST forcing in the southeast tropical Atlantic and southwest subtropical Indian Oceans. *Int J Climatol* 29:1001–1012. <https://doi.org/10.1002/joc.1919>
- Harlaß J, Latif M, Park W (2018) Alleviating tropical Atlantic sector biases in the Kiel climate model by enhancing horizontal and vertical atmosphere model resolution: climatology and interannual variability. *Clim Dyn* 50:2605–2635. <https://doi.org/10.1007/s00382-017-3760-4>
- Hersbach H, Bell B, Berrisford P, Hirahara S, Horányi A, Muñoz-Sabater J et al (2020) The ERA5 global reanalysis. *Q J R Meteorol Soc* 146:1999–2049. <https://doi.org/10.1002/qj.3803>
- Hirst AC, Hastenrath S (1983) Atmosphere-ocean mechanisms of climate anomalies in the angola-tropical Atlantic sector. *J Phys Oceanogr* 13(7):1146–1157. https://journals.ametsoc.org/view/journals/phoc/13/7/1520-0485_1983_013_1146_aomoca_2_0_co_2.xml
- Hourdin F, Gäinusă-Bogdan A, Braconnot P, Dufresne J-L, Traore A-K, Rio C (2015) Air moisture control on ocean surface temperature, hidden key to the warm bias enigma. *Geophys Res Lett* 42:10885–10893. <https://doi.org/10.1002/2015GL066764>
- Hu Z-Z, Huang B (2007) Physical processes associated with tropical Atlantic SST gradient during the anomalous evolution in the southeastern ocean. *J Clim* 20:3366–3378. <https://doi.org/10.1175/JCLI4189.1>
- Illig S, Dewitte B, Ayoub N, Du Penhoat Y, Reverdin G, De M et al (2004) Interannual long equatorial waves in the tropical Atlantic from a high-resolution ocean general circulation model experiment in 1981–2000. *J Geophys Res* 109:C02022. <https://doi.org/10.1029/2003JC001771>
- Illig S, Cadier E, Bachèlery M-L, Kersalé M (2018a) Subseasonal coastal-trapped wave propagations in the southeastern Pacific and Atlantic Oceans: 1. A new approach to estimate wave amplitude. *J Geophys Res Oceans* 123:3915–3941. <https://doi.org/10.1029/2017JC013539>
- Illig S, Bachèlery M-L, Cadier E (2018b) Subseasonal coastal-trapped wave propagations in the southeastern Pacific and Atlantic Oceans: 2. Wave characteristics and connection with the equatorial variability. *J Geophys Res Oceans* 123:3942–3961. <https://doi.org/10.1029/2017JC013540>
- Illig S, Bachèlery M-L, Lübbecke JF (2020) Why do Benguela Niños lead Atlantic Niños? *J Geophys Res Oceans* 125:e2019JC016003. <https://doi.org/10.1029/2019JC016003>
- Imbol Koungue RA, Brandt P (2021) Impact of intraseasonal waves on Angolan warm and cold events. *J Geophys Res Oceans* 126:e2020JC017088. <https://doi.org/10.1029/2020JC017088>
- Imbol Koungue RA, Illig S, Rouault M (2017) Role of interannual Kelvin wave propagations in the equatorial Atlantic on the Angola Benguela current system. *J Geophys Res Oceans* 122:4685–4703. <https://doi.org/10.1002/2016JC012463>
- Imbol Koungue RA, Rouault M, Illig S, Brandt P, Jouanno J (2019) Benguela Niños and Benguela Niñas in forced ocean simulation from 1958 to 2015. *J Geophys Res Oceans* 124:5923–5951. <https://doi.org/10.1029/2019JC015013>
- Imbol Koungue RA, Brandt P, Lübbecke J, Prigent A, Martins MS, Rodrigues RR (2021) The 2019 Benguela Niño. *Front Mar Sci* 8:800103. <https://doi.org/10.3389/fmars.2021.800103>
- Junker T, Mohrholz V, Siegfried L, van der Plas A (2017) Seasonal to interannual variability of water mass characteristics and currents on the Namibian shelf. *J Mar Syst* 165:36–46. <https://doi.org/10.1016/j.jmarsys.2016.09.003>
- Keenlyside NS, Latif M (2007) Understanding equatorial Atlantic interannual variability. *J Clim* 20:131–142. <https://doi.org/10.1175/JCLI3992.1>
- Kinnison DE, Brasseur GP, Walters S, Garcia RR, Marsh DR, Sassi F, Harvey VL, Randall CE, Emmons L, Lamarque JF, Hess P, Orlando JJ, Tie XX, del Ran- W, Pan LL, Gettelman A, Granier C, Diehl T, Niemeier U, Simmons AJ (2007) Sensitivity of chemical tracers to meteorological parameters in the MOZART-3 chemical transport model. *J Geophys Res Atmos* 112:D20302. <https://doi.org/10.1029/2006JD007879>
- Kohyama T, Hartmann DL, Battisti DS (2018) Weakening of nonlinear ENSO under global warming. *Geophys Res Lett* 45:8557–8567. <https://doi.org/10.1029/2018GL079085>
- Koseki S, Imbol Koungue RA (2020) Regional atmospheric response to the Benguela Niñas. *Int J Climatol*. <https://doi.org/10.1002/joc.6782>
- Kurian J, Li P, Chang P et al (2021) Impact of the Benguela coastal low-level jet on the southeast tropical Atlantic SST bias in a regional ocean model. *Clim Dyn* 56:2773–2800. <https://doi.org/10.1007/s00382-020-05616-5>
- Li X, Tan W, Hu Z-Z, Johnson NC (2023) Evolution and prediction of two extremely strong Atlantic Niños in 2019–2021: Impact of Benguela warming. *Geophys Res Lett* 50:e2023GL104215. <https://doi.org/10.1029/2023GL104215>
- Lübbecke JF, Böning CW, Keenlyside NS, Xie S-P (2010) On the connection between Benguela and equatorial Atlantic Niños and the role of the South Atlantic Anticyclone. *J Geophys Res* 115:C09015. <https://doi.org/10.1029/2009JC005964>
- Lübbecke JF, Brandt P, Dengler M, Kopte R, Lüdtke J, Richter I et al (2019) Causes and evolution of the southeastern tropical Atlantic warm event in early 2016. *Clim Dyn* 53:261–274. <https://doi.org/10.1007/s00382-018-4582-8>
- Madec G, and the NEMO team (2016) NEMO ocean engine—version 3.6, Note du Pôle de modélisation, Institut Pierre-Simon Laplace (IPSL), France, p 406
- Maes C, O’Kane TJ (2014) Seasonal variations of the upper ocean salinity stratification in the Tropics. *J Geophys Res Oceans* 119:1706–1722. <https://doi.org/10.1002/2013JC009366>
- Matthes K, Funke B, Andersson ME, Barnard L, Beer J, Charbonneau P, Ciliverd MA, Dudok de Wit T, Haberleiter M, Hendry A, Jackman CH, Kretzschmar M, Kruschke T, Kunze M, Langematz U, Marsh DR, Maycock AC, Misios S, Rodger CJ, Scaife AA, Sepp A, Shangguan M, Sinnhuber M, Tourpali K, Usoskin I, van de Kamp M, Verronen PT, Versick S (2017) Solar forcing for CMIP6 (v3.2). *Geosci Model Dev* 10:2247–2302. <https://doi.org/10.5194/gmd-10-2247-2017>
- Matthes K, Biastoch A, Wahl S, Harlaß J, Martin T, Brücher T, Drews A, Ehlert D, Getzlaff K, Krüger F, Rath W, Scheinert M, Schwarzkopf FU, Bayr T, Schmidt H, Park W (2020) The Flexible Ocean and Climate Infrastructure version 1 (FOCI1): mean state and variability. *Geosci Model Dev* 13:2533–2568. <https://doi.org/10.5194/gmd-13-2533-2020>
- Milinski S, Bader J, Haak H, Siongco AC, Jungclaus JH (2016) High atmospheric horizontal resolution eliminates the wind-driven coastal warm bias in the southeastern tropical Atlantic. *Geophys Res Lett* 43:10455–10462. <https://doi.org/10.1002/2016GL070530>
- O’Neill BC, Tebaldi C, van Vuuren D, Eyring V, Friedlingstein P, Hurtt G, Knutti R, Kriegler E, Lamarque JF, Lowe J, Meehl J, Moss R, Riahi K, Sanderson BM (2016) The scenario model intercomparison project (ScenarioMIP) for CMIP6 Geosci. Model Dev Discuss. <https://doi.org/10.5194/gmd-2016-84>
- Park W, Latif M (2020) Resolution dependence of CO₂-induced Tropical Atlantic sector climate changes. *Npj Clim Atmos Sci* 3:36. <https://doi.org/10.1038/s41612-020-00139-6>

- Polo I, Lazar A, Rodriguez-Fonseca B, Arnault S (2008) Oceanic Kelvin waves and tropical Atlantic intraseasonal variability: 1. Kelvin wave characterization. *J Geophys Res* 113:C07009. <https://doi.org/10.1029/2007JC004495>
- Prigent A, Imbol Koungue RA, Lübbecke JF, Brandt P, Latif M (2020a) Origin of weakened interannual sea surface temperature variability in the southeastern tropical Atlantic Ocean. *Geophys Res Lett* 47:e2020GL08348. <https://doi.org/10.1029/2020GL089348>
- Prigent A, Lübbecke JF, Bayr T, Latif M, Wengel C (2020b) Weakened SST variability in the tropical Atlantic Ocean since 2000. *Clim Dyn* 54:2731–2744. <https://doi.org/10.1007/s00382-020-05138-0>
- Rayner NA, Parker DE, Horton EB, Folland CK, Alexander LV, Rowell DP et al (2003) Global analyses of sea surface temperature, sea ice, and night marine air temperature since the late nineteenth century. *J Geophys Res* 108(D14):4407. <https://doi.org/10.1029/2002JD002670>
- Richter I (2015) Climate model biases in the eastern tropical oceans: causes, impacts and ways forward. *Wires Clim Change* 6:345–358. <https://doi.org/10.1002/wcc.338>
- Richter I, Tokinaga H (2020) An overview of the performance of CMIP6 models in the tropical Atlantic: mean state, variability, and remote impacts. *Clim Dyn* 55:2579–2601. <https://doi.org/10.1007/s00382-020-05409-w>
- Richter I, Behera SK, Masumoto Y, Taguchi B, Komori N, Yamagata T (2010) On the triggering of Benguela Niños: Remote equatorial versus local influences. *Geophys Res Lett* 37:L20604. <https://doi.org/10.1029/2010GL044461>
- Richter I, Tokinaga H, Okumura YM (2022) The extraordinary equatorial Atlantic warming in late 2019. *Geophys Res Lett* 49:e2021GL095918. <https://doi.org/10.1029/2021GL095918>
- Rouault M (2012) Bi-annual intrusion of tropical water in the northern Benguela upwelling. *Geophys Res Lett* 39:L12606. <https://doi.org/10.1029/2012GL052099>
- Rouault M, Florenchie P, Fauchereau N, Reason CJC (2003) South East tropical Atlantic warm events and southern African rainfall. *Geophys Res Lett* 30(5):8009. <https://doi.org/10.1029/2002GL014840>
- Rouault M, Illig S, Bartholomae C, Reason CJC, Bentamy A (2007) Propagation and origin of warm anomalies in the Angola Benguela upwelling system in 2001. *J Mar Syst* 68(3–4):473–488. <https://doi.org/10.1016/j.jmarsys.2006.11.010>
- Rouault M, Illig S, Lübbecke J, Imbol K, Koungue RA (2018) Origin, development and demise of the 2010–2011 Benguela Niño. *J Mar Syst* 188:39–48. <https://doi.org/10.1016/j.jmarsys.2017.07.007>
- Schultz MG, Stadtler S, Schröder S, Taraborrelli D, Franco B, Krefting J, Henrot A, Ferrachat S, Lohmann U, Neubauer D, Siegenthaler-Le Drian C, Wahl S, Kokkola H, Kühn T, Rast S, Schmidt H, Stier P, Kinnison D, Tyndall GS, Orlando JJ, Wespes C (2018) The chemistry–climate model ECHAM6.3-HAM2.3-MOZ1.0. *Geosci Model Dev* 11:1695–1723. <https://doi.org/10.5194/gmd-11-1695-2018>
- Schulzweida U (2022) CDO User Guide (2.1.0). Zenodo. <https://doi.org/10.5281/zenodo.7112925>
- Schwarzkopf FU, Biastoch A, Böning CW, Chanut J, Durgadoo JV, Getzlaff K, Harlaß J, Rieck JK, Roth C, Scheinert MM, Schubert R (2019) The INALT family—a set of high-resolution nests for the Agulhas Current system within global NEMO ocean/sea-ice configurations. *Geosci Model Dev* 12:3329–3355. <https://doi.org/10.5194/gmd-12-3329-2019>
- Shannon LV, Boyd AJ, Brundrit GB, Taunton-Clark J (1986) On the existence of an El Niño-type phenomenon in the Benguela system. *J Mar Res* 44:495–520. <https://doi.org/10.1357/002224086788403105>
- Small RJ, Curchitser E, Hedstrom K, Kauffman B, Large WG (2015) The Benguela upwelling system: quantifying the sensitivity to resolution and coastal wind representation in a global climate model. *J Clim* 28:9409–9432. <https://doi.org/10.1175/JCLI-D-15-0192.1>
- Steele M, Morley R, Ermold W (2001) PHC: a global ocean hydrography with a high-quality Arctic ocean. *J Clim* 14:2079–2087
- Stevens B, Giorgetta M, Esch M, Mauritsen T, Crueger T, Rast S, Salzmann M, Schmidt H, Bader J, Block K, Brokopf R, Fast I, Kinne S, Kornbluh L, Lohmann U, Pin-cus R, Reichler T, Roeckner E (2013) Atmospheric component of the MPI-M Earth System Model: ECHAM6. *J Adv Model Earth Syst* 5:146–172. <https://doi.org/10.1002/jame.20015>
- Tokinaga H, Xie SP (2011) Weakening of the equatorial Atlantic cold tongue over the past six decades. *Nat Geosci* 4(4):222–226. <https://doi.org/10.1038/ngeo1078>
- Valcke S (2013) The OASIS3 coupler: a European climate modelling community software. *Geosci Model Dev* 6:373–388. <https://doi.org/10.5194/gmd-6-373-2013>
- Wahl S, Latif M, Park W et al (2011) On the Tropical Atlantic SST warm bias in the Kiel Climate Model. *Clim Dyn* 36:891–906. <https://doi.org/10.1007/s00382-009-0690-9>
- Worou K, Goosse H, Fichefet T, Kucharski F (2022) Weakened impact of the Atlantic Niño on the future equatorial Atlantic and Guinean coast rainfall. *Earth Syst Dyn Discuss* 2021:1–45. <https://doi.org/10.5194/esd-2021->
- Xiang B, Wang B, Ding Q et al (2012) Reduction of the thermocline feedback associated with mean SST bias in ENSO simulation. *Clim Dyn* 39:1413–1430. <https://doi.org/10.1007/s00382-011-1164-4>
- Yang Y, Wu L, Cai W et al (2022) Suppressed Atlantic Niño/Niña variability under greenhouse warming. *Nat Clim Chang* 12:814–821. <https://doi.org/10.1038/s41558-022-01444-z>
- Zuo H, Balmaseda MA, Tietsche S, Mogensen K, Mayer M (2019) The ECMWF operational ensemble reanalysis–analysis system for ocean and sea ice: a description of the system and assessment. *Ocean Sci* 15:779–808. <https://doi.org/10.5194/os-15-779-2019>

Publisher's Note Springer Nature remains neutral with regard to jurisdictional claims in published maps and institutional affiliations.